Cellular/Molecular

AKAP150-Anchored Calcineurin Regulates Synaptic Plasticity by Limiting Synaptic Incorporation of Ca^{2+}-Permeable AMPA Receptors

Jennifer L. Sanderson,[1] Jessica A. Gorski,[1] Emily S. Gibson,[1] Philip Lam,[1] Ronald K. Freund,[1] Wallace S. Chick,[2] and Mark L. Dell'Acqua[1,3]

Departments of [1]Pharmacology and [2]Cell and Developmental Biology, and [3]Program in Neuroscience, University of Colorado School of Medicine, Aurora, Colorado 80045

AMPA receptors (AMPARs) are tetrameric ion channels assembled from GluA1–GluA4 subunits that mediate the majority of fast excitatory synaptic transmission in the brain. In the hippocampus, most synaptic AMPARs are composed of GluA1/2 or GluA2/3 with the GluA2 subunit preventing Ca^{2+} influx. However, a small number of Ca^{2+}-permeable GluA1 homomeric receptors reside in extrasynaptic locations where they can be rapidly recruited to synapses during synaptic plasticity. Phosphorylation of GluA1 S845 by the cAMP-dependent protein kinase (PKA) primes extrasynaptic receptors for synaptic insertion in response to NMDA receptor Ca^{2+} signaling during long-term potentiation (LTP), while phosphatases dephosphorylate S845 and remove synaptic and extrasynaptic GluA1 during long-term depression (LTD). PKA and the Ca^{2+}-activated phosphatase calcineurin (CaN) are targeted to GluA1 through binding to A-kinase anchoring protein 150 (AKAP150) in a complex with PSD-95, but we do not understand how the opposing activities of these enzymes are balanced to control plasticity. Here, we generated AKAP150ΔPIX knock-in mice to selectively disrupt CaN anchoring *in vivo*. We found that AKAP150ΔPIX mice lack LTD but express enhanced LTP at CA1 synapses. Accordingly, basal GluA1 S845 phosphorylation is elevated in AKAP150ΔPIX hippocampus, and LTD-induced dephosphorylation and removal of GluA1, AKAP150, and PSD-95 from synapses are impaired. In addition, basal synaptic activity of GluA2-lacking AMPARs is increased in AKAP150ΔPIX mice and pharmacologic antagonism of these receptors restores normal LTD and inhibits the enhanced LTP. Thus, AKAP150-anchored CaN opposes PKA phosphorylation of GluA1 to restrict synaptic incorporation of Ca^{2+}-permeable AMPARs both basally and during LTP and LTD.

Introduction

Long-term potentiation (LTP) and long-term depression (LTD) at hippocampal CA1 synapses are widely studied due to their involvement in learning and memory processes that are impaired in disorders including schizophrenia, Down syndrome, and Alzheimer's (Siarey et al., 1999; Miyakawa et al., 2003; Hsieh et al., 2006; Shankar et al., 2007; Scott-McKean and Costa, 2011). LTP and LTD are induced by Ca^{2+} influx through postsynaptic NMDA receptors (NMDARs) and expressed by long-lasting increases or decreases, respectively, in AMPA receptor (AMPAR) function. Phosphorylation of AMPAR GluA1 (formerly GluR1) subunits on S845 by the cAMP-dependent protein kinase (PKA) increases channel open probability and promotes receptor recycling and exocytosis at extrasynaptic sites near the postsynaptic density (PSD) (Banke et al., 2000; Ehlers, 2000; Esteban et al., 2003; Oh et al., 2006; Man et al., 2007; Yang et al., 2008; He et al., 2009). Extrasynaptic AMPARs can move into the PSD in response to PKC and CaMK activation during LTP (Oh et al., 2006; Guire et al., 2008; Makino and Malinow, 2009; Petrini et al., 2009; Opazo et al., 2010; Yang et al., 2010), while protein phosphatases PP1, PP2A, and calcineurin (CaN) (also known as PP2B) dephosphorylate GluA1 S845 and remove receptors by endocytosis during LTD (Mulkey et al., 1993; Kameyama et al., 1998; Lee et al., 1998, 2000, 2003, 2010; Beattie et al., 2000; Ashby et al., 2004).

Recent studies indicate that S845 phosphorylation stabilizes Ca^{2+}-permeable GluA1 receptors lacking GluA2 in extrasynaptic locations where they are dephosphorylated during LTD (He et al., 2009). Importantly, forms of LTP that are regulated by PKA also involve GluA2-lacking receptors and S845 phosphorylation (Esteban et al., 2003; Lee et al., 2003, 2010; Lu et al., 2007; Yang et al., 2010; Qian et al., 2012). Thus, a key question is how are PKA and

Received July 12, 2012; revised Aug. 21, 2012; accepted Aug. 28, 2012.

Author contributions: J.L.S., J.A.G., E.S.G., R.K.F., W.S.C., and M.L.D. designed research; J.L.S., J.A.G., E.S.G., P.L., R.K.F., W.S.C., and M.L.D. performed research; J.L.S., J.A.G., E.S.G., P.L., R.K.F., and M.L.D. analyzed data; J.L.S. and M.L.D. wrote the paper.

This work was supported by National Institutes of Health (NIH)–National Institute of Neurological Disorders and Stroke (NINDS) Grant R01 NS040701 (M.L.D.). J.L.S. was supported by NIH–National Institute on Alcohol Abuse and Alcoholism Grant T32AA007464 and an American Heart Association postdoctoral fellowship. AKAP150ΔPIX knock-in mice were generated using the NIH–NINDS-supported Rocky Mountain Neurological Disorders Core Center (Grant P30NS048154). Confocal microscopy on brain slices was performed in the University of Colorado Anschutz Medical Campus Advanced Light Microscopy Core supported by the Rocky Mountain Neurological Disorders Core Center (Grant P30NS048154) and NIH–National Center for Research Resources Colorado Clinical and Translational Sciences Institute (Grant UL1RR025780). Contents are the authors' sole responsibility and do not necessarily represent official NIH views. We thank Dr. Karen Smith for assistance with breeding and initial characterization of AKAP150ΔPIX mice during the early stages of this work. We thank Drs. K. Ulrich Bayer, Matthew Kennedy, and Timothy A. Benke for critical reading of this manuscript.

Correspondence should be addressed to Mark L. Dell'Acqua, Department of Pharmacology, University of Colorado Anschutz Medical Campus, 12800 East 19th Avenue, Mail Stop 8303, Aurora, CO 80045. E-mail: mark.dellacqua@ucdenver.edu.

DOI:10.1523/JNEUROSCI.3326-12.2012

 0270-6474/12/3215036-17$15.00/0

phosphatases such as CaN targeted to synapses to regulate GluA1 during LTP and LTD?

Human AKAP79 and its rodent ortholog AKAP150 are postsynaptic scaffold proteins that anchor PKA and CaN (Sanderson and Dell'Acqua, 2011). Past studies using *in vitro* cultures implicated AKAP79/150 in regulation of AMPAR phosphorylation, activity, and trafficking (Colledge et al., 2000; Gomez et al., 2002; Tavalin et al., 2002; Hoshi et al., 2005; Smith et al., 2006; Bhattacharyya et al., 2009; Keith et al., 2012). In particular, a recent study in cultured rat hippocampal slices using RNAi identified a requirement for AKAP150-CaN anchoring in LTD (Jurado et al., 2010), while independent work on hippocampal slices from PKA-anchoring deficient AKAP150D36 knock-in mice found impacts on both LTD and LTP (Lu et al., 2007, 2008). However, we do not know whether AKAP150-anchored CaN regulates LTP or LTD *in vivo* or understand the underlying mechanisms in sufficient detail. Thus, here we generated AKAP150ΔPIX knock-in mice with a deletion of the conserved PxIxIT-like CaN anchoring motif (Dell'Acqua et al., 2002; Oliveria et al., 2007) to eliminate CaN anchoring *in vivo*. Importantly, using AKAP150ΔPIX mice we found that anchored CaN limits GluA1 phosphorylation and Ca^{2+}-permeable AMPAR recruitment to synapses to promote LTD and constrain LTP.

Materials and Methods

Animal use and care. All animal procedures were conducted in accordance with National Institutes of Health (NIH)–United States Public Health Service guidelines and with the approval of the University of Colorado, Denver, Institutional Animal Care and Use Committee.

Generation of AKAP150ΔPIX knock-in mice. The Rocky Mountain Neurological Disorders Gene Targeting Core constructed the *akap5*ΔPIX targeting vector. The ΔPIX mutation, which removes 21 bp encoding 655-PIAIIIT-661, was introduced into the single coding exon of an *akap5* genomic DNA fragment subcloned from a C57BL/6 BAC clone. In this targeting vector, the ΔPIX mutation and a C-terminal myc-epitope tag were introduced by PCR along with a neomycin resistance cassette flanked by loxP sites inserted into 3′ genomic DNA. The targeting construct was electroporated into a hybrid C57BL/6129 embryonic stem (ES) cell and G418-resistant clones were screened for homologous recombinants by PCR-based genotyping. One positive clone was expanded, injected into blastocysts, and implanted into surrogate mothers. Chimeric F_0 founders were born and bred to C57BL/6 to establish germ-line transmission. F_1 mice heterozygous for the AKAP150ΔPIX mutation were identified and then bred to yield F_2 AKAP150ΔPIX homozygous offspring. For PCR genotyping, DNA was extracted from tail snips using REDExtract-N-Amp Tissue PCR kit (Sigma-Aldrich) following manufacturer's recommendations. PCR with forward (5′-AGAAGA AAGCAAACGAATGGA-3′) and reverse (5′-TGCTCGTTTTCCATTG AAATTA-3′) primers amplified nucleotides 1869–1991 of the coding sequence, giving a 122 bp fragment for the wild-type (WT) allele and a 101 bp fragment for the ΔPIX allele. For most experiments, AKAP150ΔPIX mice were maintained on a mixed C57BL/6129 background as heterozygous breeding pairs to provide WT littermate controls; however, for neonatal cultured neuron preparations, WT and ΔPIX homozygous breeding pairs were used to provide litters of a single genotype. AKAP150ΔPIX mice have no obvious alterations in physical, behavioral, or breeding phenotype in the home cage environment.

Subcellular fractionation of hippocampal tissue. Fractionation was performed as per Smith et al. (2006), with slight modifications. Whole hippocampi from 2- to 3-week-old mice were homogenized in 500 ml of homogenization buffer [10 mM Tris base, pH 7.6, 320 mM sucrose, 150 mM NaCl, 5 mM EDTA, 5 mM EGTA, 1 mM benzamidine, 1 mM 4-(2-aminoethyl)benzenesulfonyl fluoride, 2 μg/ml leupeptin, 2 μg/ml pepstatin, and 50 mM NaF] by 30 strokes in a Dounce homogenizer. The homogenates were centrifuged at 960 × *g* to remove nuclei and large debris. Crude synaptosomal membranes (P2) were prepared from supernatants by centrifugation at 10,000 × *g*. The P2 pellet was resuspended in homogenization buffer, and an aliquot was taken for immunoblotting analysis. Crude PSD fractions (TxP) were generated by incubating the remaining P2 sample on ice in homogenization buffer plus 0.5% Triton X-100 for 20 min followed by centrifugation at 32,000 × *g*. Final pellets were sonicated in resuspension buffer (10 mM Tris, pH 8, 1 mM EDTA, and 1% SDS). Protein concentrations were determined using the BCA Protein Assay kit (Pierce), according to manufacturer's directions.

Immunoprecipitation and immunoblotting. AKAP150 immunoprecipitations from the hippocampus of ~2-month-old male and female mice were performed as per Gomez et al. (2002) with slight modifications. Hippocampi were homogenized in lysis buffer (50 mM Tris, pH 7.5, 0.15 M NaCl, 5 mM EDTA, 5 mM EGTA, 5 mM NaF, 2 mg/ml leupeptin, 2 mg/ml pepstatin, 1 mM benzamidine, and 1 mM AEBSF [4-(2-aminoethyl)benzenesulfonyl fluoride]), and then incubated on ice for 20 min in the presence of 1% Triton X-100 and 0.5% deoxycholate. Lysates were spun for 20 min at 20,800 × *g*. Ten percent of supernatant was reserved for gel loading. The remaining supernatant was diluted to 0.5% Triton X-100 and 0.25% deoxycholate and split evenly into two samples, receiving either 5 μg of rabbit anti-AKAP150 or 5 μg of rabbit anti-IgG antibodies. Samples were incubated for 4 h at room temperature with end-over-end shaking, followed by 1 h in protein A-Sepharose beads, before extensive washing.

The entire immunoprecipitates, 15 μg of whole extract (WE/input), 10 μg of P2, 20 μg of S2, 5 μg of TxP, and 15 μg of TxS were resolved on Tris-SDS gels and transferred in 20% methanol to PVDF membranes. Forty micrograms of WE were loaded on the gel for parallel blotting with anti-myc and anti-AKAP150. Primary antibodies were incubated with the membranes for a minimum of 90 min as follows: rabbit anti-AKAP150 (1:2000) (Brandao et al., 2012), mouse anti-myc and anti-PKA-RIIα (1:1000; Santa Cruz Biotechnology), mouse anti-PKA-C, mouse-anti-N-cadherin and mouse anti-PKA-RIIβ (1:1000; BD Biosciences Transduction Laboratories), mouse anti-pan-PSD-MAGUK family, mouse anti-calcineurin A (1:1000; Sigma-Aldrich), mouse anti-PSD-95 (1:1000; NeuroMab), rabbit anti-GluA2/3 (1:1000; Millipore), rabbit anti-GluA1 (1:1000; Calbiochem; EMD-Millipore). For pS845 GluA1 immunoblotting analysis in both hippocampal tissue and acute hippocampal slice, 15 μg of WE extract was loaded on gels and blots were probed first overnight at 4°C with rabbit anti-GluA1-S845 (1:500–1000; Millipore) followed by stripping and reprobing of the same blots overnight at 4°C with rabbit anti-GluA1, as above, to detect total receptor levels. Detection was performed with HRP-coupled secondary antibodies (Bio-Rad; 1:1000) followed by ECL (West Pico or West Dura Chemiluminescent Substrate; Pierce). Chemiluminescence was imaged using an Alpha Innotech Fluorchem gel documentation system, and band intensities were analyzed using ImageJ software (NIH). For subcellular fractionation experiments, band intensities were expressed as a fraction of the intensity obtained for the WT WE for that given blot.

Immunohistochemistry on acute hippocampal slices. Two- to 3-week-old male and female mice were decapitated under deep anesthesia with ketamine (250 mg/kg, i.p.). Acute coronal 300 μm brain slices were prepared in 4°C cutting solution (in mM: 3 KCl, 1.25 NaH_2PO_4, 12 $MgSO_4$, 26 $NaHCO_3$, 0.2 $CaCl_2$, 220 sucrose, 10 glucose) (Shuttleworth and Connor, 2001) using a Vibratome. Slices were transferred to a mixture of cutting solution and ACSF (in mM: 126 NaCl, 3 KCl, 2 $CaCl_2$, 1.25 NaH_2PO_4, 1 $MgSO_4$, 26 $NaHCO_3$, 10 glucose; osmolarity, 300 mOsm) saturated with 95% O_2 and 5% CO_2 at room temperature and recovered for >80 min. Slices were fixed in 4% paraformaldehyde at 4°C for 24 h and processed for immunostaining as described by Hoskison et al. (2007). Briefly, slices were incubated in PBS plus 0.1% TX-100 and 2% BSA with primary antibodies [rabbit anti-AKAP150, 1:500, and mouse anti-CaN B, 1:500 (Millipore)] for 48 h, with a solution change after 24 h. Slices were washed in PBS for an extended period of time and incubated in secondary antibodies overnight at 4°C (goat anti-rabbit Alexa 488, 1:500; and goat anti-mouse Texas Red, 1:500; Invitrogen). Following another extended wash, the slices were stained with DAPI (1:500; Invitrogen) for 10 min, washed, and then mounted onto glass slides using Vectashield (Vector Laboratories).

Golgi staining and spine counting. Golgi staining of brains from 2- to 3-week-old male and female mice was performed as per manufacturer's instructions using FD Rapid GolgiStain Kit (FD Neurotechnologies). Briefly, 2- to 3-week-old male and female mice were killed by decapitation while under isoflurane anesthesia, and brains were removed rapidly, rinsed briefly in water, and placed in impregnation solution (mixture of Golgi solutions A and B) for 14 d in the dark at room temperature; the impregnation mixture was replaced once after 12–24 h. The brains were transferred into Golgi solution C and stored at 4°C in the dark for 2–12 d; Golgi solution C was replaced after 12–24 h. Brains were mounted with minimal amounts of OCT and frozen in dry ice. Sections (80 μm) were cut on a cryostat (at −23°C) and slices were mounted on gelatin-coated slides in a drop of Golgi solution C and allowed to dry in the dark at room temperature for 24 h. Sections were then stained using Golgi solutions D and E, dehydrated in ethanol followed by xylene, and mounted in Permount (Thermo Fisher Scientific). Slides were stored at room temperature in the dark until imaging.

Golgi-stained apical dendrites of CA1 pyramidal neurons were imaged by transmitted light on a Zeiss Axiovert 200M microscope, using a 63× Plan-Apo/1.4 NA objective and a Coolsnap CCD camera (Photometrics) operated by Slidebook 5.0 software (Intelligent Imaging Innovations). Spines were counted from image stacks using ImageJ (NIH) for 20–105 μm segments of secondary or higher-order dendrites >40 μm from the cell body. Counts are expressed as spines/micrometer for three mice per genotype with seven to eight neurons from different sections along the rostral-caudal axis analyzed per mouse and between one and four dendritic segments counted and averaged per neuron.

Extracellular field recordings. Two- to 3-week-old male and female mice were decapitated, and the brain was quickly removed into 4°C cutting solution. The hippocampi were removed from the brain, and 400-μm-thick slices were made using a McIIwain tissue chopper. Slices were recovered at 31°C for >80 min in ACSF (in mM: 126 NaCl, 3 KCl, 2 $CaCl_2$, 1.25 NaH_2PO_4, 1 $MgSO_4$, 26 $NaHCO_3$, 10 glucose). Following recovery, a bipolar tungsten stimulating electrode was placed in the Schaffer collateral (SC) pathway 200–300 μm from CA1 cell bodies to evoke fEPSPs recorded in the stratum radiatum using a nearby glass micropipette filled with ACSF (access resistance, 2–5 MΩ). Input–output curves were measured by evoking fEPSPs at different intensities until maximal stimulation was determined by plotting fEPSP slope against stimulus intensity. For studies of LTP and LTD, the test stimulus intensity was set to evoke 40–60% of the maximum slope and delivered at 0.05 Hz. *N*,*N*,*H*,-trimethyl-5-[(tricyclo[3.3.1.13,7]dec-1-ylmethyl)amino]-1-pentanaminiumbromide hydrobromide (IEM1460) was purchased from Tocris. Scope54 software was used for data acquisition and analysis.

Whole-cell electrophysiology. For whole-cell voltage-clamp electrophysiological recordings, 300 μm hippocampal slices were prepared using a Vibratome. After >80 min recovery, slices were transferred to a recording chamber and maintained at 31°C and visualized using infrared–differential interference contrast microscopy. Patch-clamp electrodes had a resistance between 3 and 6 MΩ. Voltage-clamp recordings were obtained using an Axopatch 200B amplifier (Molecular Devices) at a holding potential of −65 mV except as noted below for AMPAR/NMDAR evoked EPSC (eEPSC) ratios and AMPAR rectification measurements. AMPAR sEPSCs were recorded from CA1 pyramidal neurons using an intracellular solution containing the following (in mM): 140 CsCl, 10 HEPES, 1 EGTA, 4 MgATP, 0.4 MgGTP, and 1.5 QX-314, pH 7.3, and were isolated using 50 μM picrotoxin (Tocris) with further isolation of mEPSCs in 0.5 μM TTX (Tocris). $GABA_A$ receptor sIPSCs were recorded using the same internal solution, but were isolated using 10 μM NBQX (Tocris) with further isolation of mIPSCs in 0.5 μM TTX. Evoked eEPSCs were recorded in whole-cell configuration. Half-maximum stimulation was determined, and then currents were evoked at holding potentials of either −65 mV (inward AMPAR current) or +40 mV (outward AMPAR plus NMDAR current). Averaging recorded events (>10/neuron) and overlaying the traces at −65 mV and +40 was used to measure AMPA/NMDA current ratios as follows: AMPAR currents at +40 or −65 mV were measured from the peak amplitude of the EPSC and divided by NMDAR currents at +40 mV measured 70 ms after the onset of the EPSC, by which time the AMPAR component had largely decayed as monitored by recording at −65 mV. Normalized AMPAR eEPSC *I–V* curves were obtained from averaged recordings (>10/neuron) in the presence of 10 μM MK-801 extracellularly (Tocris) and 10 μM spermine intracellularly. Normalized *I–V* plots were generated from measurements of AMPAR eEPSC peak amplitudes at different membrane holding potential by dividing by the mean AMPAR eEPSC peak amplitude determined at −65 mV for each genotype. AMPAR rectification values were obtained by dividing the peak amplitudes of AMPAR eEPSCs recorded at −65 mV by those recorded at +40 mV for each neuron as in the study by Stubblefield and Benke (2010).

Analysis of GluA1 Ser845 phosphorylation. Acute hippocampal slices were prepared as described above using a Vibratome. Slices were recovered at 31°C for >120 min, and then the CA3 region was removed. Slices were exposed to 20 μM NMDA for 3 min at 31°C, washed in ASCF, and recovered for different times. Multiple slices were collected for each time point and sonicated in buffer (1% SDS, 10 mM EDTA, 100 mM Tris, pH 8). This homogenate was heated to 95°C for 5 min and then frozen at −70°C until SDS-PAGE and immunoblotting (see above) with anti-phospho-S845 GluA1 followed by stripping and reprobing of the same blots with anti-GluA1 to detect total receptor levels. For basal GluA1 pS845 analysis, band intensities for pS845 were normalized to the total GluA1 intensity for the same band to give a normalized pS845/GluA1 ratio. For time course analysis after NMDA–chemical LTD (cLTD), pS845/GluA1 ratios were normalized to the average WT value for the $t = 0$ (untreated) condition.

Immunocytochemistry on mouse primary hippocampal neuron cultures. Mouse hippocampal neurons were cultured from postnatal day 0–2 male and female mice as previously described for rat neurons (Gomez et al., 2002; Smith et al., 2006). Briefly, the hippocampus was dissected from postnatal day 0–2 AKAP150ΔPIX or AKAP150WT mice and dissociated in papain. Neurons were plated in Neurobasal plus B27 (Invitrogen) at a medium density of 150,000–225,000 cells/ml on glass coverslips coated with poly-D-lysine and laminin (BD Biosciences) and maintained at 37°C, 5% CO_2 for 12–14 d before NMDA-cLTD experiments. For NMDAR-induced cLTD, after 12–14 d in culture, neurons were treated with 30, 50, or 70 μM NMDA for 5 min, washed, and allowed to recover for 7.5, 15, or 30 min all in culture media at 37°C, 5% CO_2. After treatments, neurons were washed with PBS, fixed in 4% paraformaldehyde, permeabilized in 0.2% Triton X-100 in PBS, and then blocked overnight in PBS plus 10% BSA. Primary antibodies were incubated for 2 h at room temperature in PBS plus 10% BSA as follows: rabbit anti-AKAP150, 1:500, or rabbit anti-GluA1, 1:500 (Millipore), and mouse anti-PSD-95, 1:500 (NeuroMab). Cells were then washed in PBS, and incubated in fluorescent secondary antibody conjugates [goat anti-rabbit Texas Red, 1:250, and goat anti-mouse Alexa 647, 1:500 (Invitrogen)] for 1 h at room temperature. Coverslips were washed and mounted onto slides with ProLong Gold (Invitrogen).

Fluorescence microscopy and image analysis. Confocal images of immunostained brain slices were obtained on an Olympus FV-1000 confocal microscope with a 60×, 1.4 NA objective at 800 × 800 pixel resolution (0.26 μm/pixel) using laser excitation at 405 nm (DAPI), 488 nm (Alexa 488), and 543 nm (Texas Red). Images of immunostained cultured neurons were obtained on a Zeiss Axiovert 200M microscope equipped with a 175W xenon lamp (Sutter), 63× Plan-Apo/1.4 NA objective, Cy3/Texas Red and Cy5/Alexa 647 filter sets (Chroma), Coolsnap CCD camera, and Slidebook 4.0–5.0 software as described previously (Gomez et al., 2002; Gorski et al., 2005; Horne and Dell'Acqua, 2007; Robertson et al., 2009). Briefly, images were acquired with 2 × 2 binning at a resolution of 696 × 520 pixels (0.21 μm/pixel) using exposure times of 150 ms for Texas Red and 500 ms for Alexa 647. Three-dimensional *z*-stack images of *x*, *y* planes with 0.5 μm steps were collected and deconvolved to the nearest neighbor to generate confocal *x*, *y* sections. Two-dimensional maximum-intensity projection images were generated from these deconvolved image stacks for quantitative mask analysis in Slidebook 4.0–5.0 to measure colocalization using Pearson's correlation (r): scale of 1, perfect correlation; 0, no correlation/random overlap; to −1, inverse correlation. The mean intensity of PSD-95 dendritic puncta was measured by defining areas of continuous pixel intensity 1.5× above the

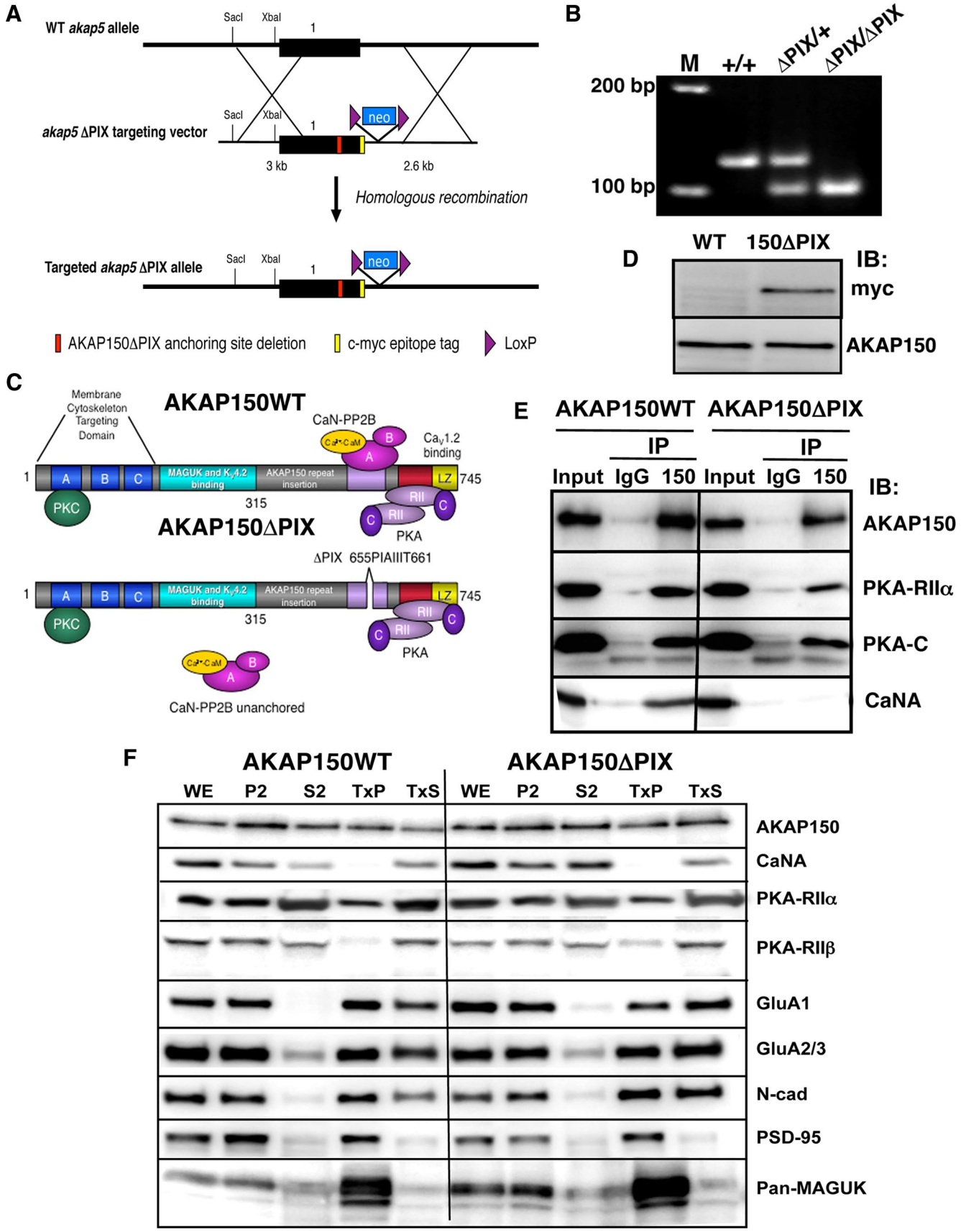

Figure 1. Generation and characterization of CaN anchoring-deficient AKAP150ΔPIX knock-in mice. ***A***, Schematics of the mouse *akap5* gene encoding the WT AKAP150 allele, the *akap5* targeting construct containing the ΔPIX mutation, and the targeted *akap5* ΔPIX allele following homologous recombination. The single AKAP150 coding exon is shown as a thick black line, and the surrounding genomic sequence as a thin black line. The red rectangle indicates the 21 bp encoding the 7 aa of the ΔPIX deletion, the yellow rectangle indicates the in-frame insertion of a c-myc epitope tag at the C-terminal end of the AKAP150 coding sequence, and the green triangles indicate loxP sites that flank the neomycin resistance (*Figure legend continues.*)

mean intensity of the dendrite as in the study by Horne and Dell'Acqua (2007). For analysis of AKAP150 and CaNB staining in single *x–y* planes from brain slices, masks were manually drawn over the CA1 cell body/soma layer and dendritic regions to obtain dendrite/soma mean intensity ratios and Pearson's correlation (*r*) values for the dendritic mask.

Full-size images were exported from Slidebook 4.0–5.0 as 8-bit TIFF images at 72 dpi resolution and assembled into figures for publication using Adobe Photoshop CS2. Maximum and minimum levels for each channel were adjusted the same amount across all images for a given staining condition. In Figures 2*F*, 8, *A* and *B*, and 9, *A* and *B*, cropping and resizing of images of dendrites to reach 300 dpi resolution in the final figures introduced some extra pixel content and image smoothing.

Statistical analysis. Group comparisons to control were performed in Prism (GraphPad) using one-way ANOVA with Dunnett's *post hoc* analysis. GluA1 S845 phosphorylation time course data were analyzed in Prism by two-way ANOVA with Bonferroni's *post hoc* analysis. For ANOVA, only $p > 0.05$ (not significant), $^{*}p < 0.05$, $^{**}p < 0.01$, and $^{***}p < 0.001$ are provided by the software. Pairwise comparisons were performed in Prism or Excel (Microsoft) using Student's *t* test, and the actual *p* values are provided. In all cases, significance is reported as $p < 0.05$, and data are expressed as mean ± SEM (error bars). Binned cumulative distributions for m/sI/EPSC recording data were generated and plotted in Prism.

Results

Generation and characterization of CaN-anchoring deficient AKAP150ΔPIX knock-in mice

Complete knock-out of AKAP150 removes multiple and opposing signaling functions in the scaffold, including both PKA and CaN anchoring, thus making mechanistic interpretations of any impacts on synaptic plasticity difficult. In general, AKAP150 knock-out mice show more limited changes in synaptic plasticity and behavior than AKAP150D36 mice, which contain a knock-in C-terminal truncation that disrupts PKA anchoring (Lu et al., 2007, 2008; Tunquist et al., 2008; Weisenhaus et al., 2010). In particular, hippocampal slices from AKAP150 knock-out mice exhibit normal LTD and LTP under the same conditions in which AKAP150D36 mice show strong deficits in both LTP and LTD, suggesting that simultaneous removal of both PKA and CaN anchoring allows compensation (Weisenhaus et al., 2010). Thus, to specifically address the role of CaN anchoring *in vivo*, we created a knock-in mouse that selectively deletes the CaN anchoring domain on AKAP150. We previously identified and structurally characterized a conserved motif, PIAIIIT, in AKAP79/150 that is a variant of the consensus PxIxIT motif found in a number of other CaN A catalytic subunit binding proteins and substrates (Dell'Acqua et al., 2002; Oliveria et al., 2007; Li et al., 2011, 2012). This motif is required for cellular anchoring of CaN, and its deletion eliminates functional regulation of L-type voltage-gated Ca^{2+} channel currents and signaling to the nucleus by CaN in cultured neurons (Oliveria et al., 2007). We generated CaN anchoring-deficient AKAP150ΔPIX mice by homologous recombination in ES cells using a targeting vector that deletes the 21 bp coding sequence for residues 655PIAIIIT661 from the mouse *akap5* gene and inserts a C-terminal myc epitope tag (Fig. 1*A*). The resulting ES cells with the targeted *akap5* ΔPIX allele were introduced into mouse embryos to create chimeric founder mice and then bred to C57BL/6 mice to obtain AKAP150ΔPIX heterozygous and homozygous offspring as detected by PCR-based genotyping compared with WT (Fig. 1*B*). Importantly, ΔPIX deletion of 655PIAIIIT661 from AKAP150 selectively eliminates CaN anchoring while leaving intact all the other AKAP structural domains and functions including PKA and PKC anchoring, membrane targeting, ion channel binding, and linkage to AMPAR and NMDAR by PSD-95 family membrane-associated guanylate kinase (MAGUK) scaffold proteins (Fig. 1*C*).

Expression of AKAP150ΔPIX protein in homozygous mice was confirmed by immunoblotting to detect the engineered C-terminal myc tag (Fig. 1*D*). Importantly, anti-AKAP150 immunoblotting showed that AKAP150ΔPIX and AKAP150WT proteins were expressed at equal levels in hippocampal extracts (Fig. 1*D–F*, Table 1), but AKAP150 immunoprecipitation revealed selective loss of CaNA, but not PKA-RII regulatory and PKA-C catalytic subunits, from the AKAP complex for ΔPIX (Fig. 1*E*). AKAP150 and a number of its known direct (PKA-RII, CaNA, N-cad, PSD-95, MAGUK) and indirect binding partners (GluA1, GluA2/3) also exhibited essentially normal expression and distribution across subcellular fractions (WE, whole tissue extracts; P2, crude synaptic membranes; S2, cytosolic fraction; TxP, crude Triton X-100-insoluble PSD fraction; TxS, Triton X-100-soluble synaptic/extrasynaptic membrane) isolated from hippocampal tissue of 2- to 3-week-old ΔPIX and WT mice (Fig. 1*F*, Table 1).

Importantly, AKAP150ΔPIX mice had no gross abnormalities in overall brain structure and anatomy. Acute hippocampal slices stained with DAPI to visualize nuclei/cell bodies revealed normal cellular organization and anatomy in the dentate gyrus and CA1 subfields (Fig. 2*A*). Additional immunostaining of slices from AKAP150ΔPIX versus WT mice (Fig. 2*B*) showed no differences in the ratios of AKAP150 or CaN distribution in dendritic regions versus the CA1 pyramidal cell body/soma layer (Fig. 2*C*: AKAP150 dendrite/soma: WT, 0.62 ± 0.07, $n = 8$; ΔPIX, 0.69 ± 0.07, $n = 10$, $p = 0.25$) (Fig. 2*D*: CaN dendrite/soma: WT, 0.85 ± 0.07, $n = 8$; ΔPIX, 0.84 ± 0.04, $n = 10$, $p = 0.46$) or relative colocalization of AKAP150 and CaN staining intensity in dendritic regions [Fig. 2*E*; AKAP/CaN correlation (*r*): WT, 0.66 ± 0.03, $n = 8$; ΔPIX, 0.69 ± 0.03, $n = 10$, $p = 0.25$]. These results showing that CaN fractionation and localization are unchanged in AKAP150ΔPIX mouse hippocampus are not surprising given that CaN is a very abundant proteins in neurons, has other binding partners both presynaptic and postsynaptic, and engages in a dynamic, modest-affinity interaction with AKAP79/150 (Li et al., 2012). Finally, we used Golgi staining to visualize dendritic spines in the hippocampus of WT and ΔPIX mice (Fig. 2*F*) and observed no differences in spine morphology or number as quantified by spine density counts (spines/10 μm: WT, 18.2 ± 0.8, $n = 12$; ΔPIX, 17.8 ± 0.6, $n = 14$; $p = 0.69$). Thus, the ΔPIX knock-in mutation has no detectable impact on overall neuronal organization or CaN expression but, as designed, selectively dissociates CaN from AKAP150 *in vivo* (Fig. 1*D*).

←

(*Figure legend continued.*) cassette in the 3′ flanking genomic DNA. ***B***, PCR-based genotyping AKAP150WT and heterozygous and homozygous AKAP150ΔPIX littermate mice to detect the 21 bp ΔPIX deletion. ***C***, Diagram of AKAP150 protein primary structure indicating removal of the PxIxIT-like 655-PIAIIIT-661 binding motif to selectively disrupt CaN-PP2B anchoring. ***D***, Detection of AKAP150ΔPIX protein in whole-cell hippocampal extracts from homozygous mice by anti-myc and anti-AKAP150 immunoblotting (IB). ***E***, The AKAP150ΔPIX mutation selectively eliminates anti-AKAP150 coimmunoprecipitation (IP) of CaNA subunits but not PKA-C or RII subunits. Input, Whole-cell hippocampal extract. ***F***, Hippocampal subcellular fractions were prepared by differential centrifugation and immunoblotted to detect multiple components of the AKAP79/150 signaling as indicated. Quantification of relative densities (see Table 1) revealed that all proteins in the complex showed essentially normal expression levels and subcellular distributions except N-cad, which was decreased 45 ± 6% in the P2 fraction for ΔPIX compared with WT ($p = 0.019$).

Table 1. Subcellular fractionation of AKAP150 signaling complex components in WT and AKAP150ΔPIX mouse hippocampus

		WT		ΔPIX		*t* test
Protein	Fraction	Mean ± SEM	*n*	Mean ± SEM	*n*	*p* value
AKAP150	WE	1 ± 0	3	1.1 ± 0.01	3	0.42
	P2	1.3 ± 0.1	3	1.4 ± 0.1	3	0.74
	S2	1 ± 0.07	3	1.1 ± 0.09	3	0.39
	TxP	1.3 ± 0.1	3	1.1 ± 0.09	3	0.19
	TxS	1.4 ± 0.3	3	1.3 ± 0.1	3	0.97
PKA-RIIα	WE	1 ± 0	6	1.1 ± 0.1	4	0.36
	P2	1 ± 0.1	6	0.84 ± 0.1	4	0.24
	S2	1.3 ± 0.2	6	0.91 ± 0.2	4	0.32
	TxP	0.63 ± 0.1	6	0.48 ± 0.1	4	0.46
	TxS	1.2 ± 0.2	6	1.1 ± 0.3	4	0.55
PKA-RIIβ	WE	1 ± 0	5	1.3 ± 0.6	4	0.66
	P2	0.75 ± 0.2	5	0.67 ± 0.06	4	0.80
	S2	0.69 ± 0.2	5	1.1 ± 0.4	4	0.30
	TxP	0.37 ± 0.1	5	0.94 ± 0.6	4	0.26
	TxS	1.7 ± 0.4	5	1.9 ± 1	4	0.81
CaNA	WE	1 ± 0	6	0.92 ± 0.06	4	0.30
	P2	0.78 ± 0.1	6	0.67 ± 0.06	4	0.52
	S2	1.5 ± 0.2	6	1.1 ± 0.3	4	0.34
	TxP	0.19 ± 0.05	6	0.087 ± 0.05	4	0.19
	TxS	0.91 ± 0.1	6	0.84 ± 0.5	4	0.85
GluA1	WE	1 ± 0	8	1.3 ± 0.1	6	0.062
	P2	1 ± 0.08	8	0.75 ± 0.1	6	0.054
	S2	0.31 ± 0.08	8	0.18 ± 0.03	6	0.20
	TxP	0.78 ± 0.05	8	0.74 ± 0.1	6	0.75
	TxS	0.83 ± 0.05	8	0.66 ± 0.2	6	0.29
GluA2/3	WE	1 ± 0	5	0.86 ± 0.06	3	0.13
	P2	0.82 ± 0.2	5	0.55 ± 0.3	3	0.41
	S2	0.23 ± 0.06	5	0.17 ± 0.1	3	0.69
	TxP	0.75 ± 0.1	5	0.97 ± 0.1	3	0.29
	TxS	0.88 ± 0.04	5	0.84 ± 0.1	3	0.70
N-cad	WE	1 ± 0	7	0.82 ± 0.1	4	0.22
	P2	1.1 ± 0.1	7	0.59 ± 0.05	4	0.019
	S2	0.19 ± 0.05	7	0.12 ± 0.07	4	0.41
	TxP	1.2 ± 0.2	7	0.86 ± 0.04	4	0.21
	TxS	0.92 ± 0.2	7	0.77 ± 0.09	4	0.50
PSD-95	WE	1 ± 0	6	0.77 ± 0.06	3	0.063
	P2	0.88 ± 0.1	6	0.56 ± 0.03	3	0.12
	S2	0.41 ± 0.1	6	0.093 ± 0.01	3	0.51
	TxP	1.4 ± 0.5	6	1 ± 0.09	3	0.59
	TxS	0.35 ± 0.1	6	0.18 ± 0.04	3	0.37
Pan-MAGUK	WE	1 ± 0	3	2.1 ± 0.5	3	0.14
	P2	1.2 ± 0.2	3	2.2 ± 0.3	3	0.071
	S2	0.94 ± 0.1	3	1.1 ± 0.1	3	0.42
	TxP	3.6 ± 1	3	7.4 ± 2	3	0.13
	TxS	0.5 ± 0.1	3	0.6 ± 0.2	3	0.73

Basal synaptic transmission is normal in AKAP150ΔPIX knock-in mice

Changes in basal synaptic transmission can impact plasticity, and a previous study found that 150RNAi combined with expression of a CaN anchoring mutant increased basal AMPAR transmission in cultured slices (Jurado et al., 2010). Thus, we evaluated whether disrupting AKAP150-CaN anchoring altered basal synaptic activity in acute hippocampal slices from ΔPIX mice. First, we recorded extracellular field EPSPs (fEPSPs) in CA1 stratum radiatum of acute slices from 2- to 3-week-old mice in response to stimulation of the SC inputs from CA3 (Fig. 3*A*). We generated input–output (I-O) curves by plotting the initial fEPSP slope in response to a range of stimulus intensities and found only small differences in I-O relationships between AKAP150ΔPIX and WT (Fig. 3*B*; 2 V: WT, 400 ± 90 mV/ms, $n = 7$; ΔPIX, 250 ± 60 mV/ms, $n = 9$, $p = 0.18$; 4 V: WT, 1860 ± 290 mV/ms, $n = 6$; ΔPIX, 1160 ± 142 mV/ms, $n = 9$, $^{*}p = 0.032$; 6 V: WT, 1770 ± 40, $n = 3$; ΔPIX, 1680 ± 240, $n = 6$, $p = 0.80$). Next, we evaluated presynaptic function and short-term plasticity by measuring paired-pulse facilitation ratios (PPRs), and found no significant differences in PPR at SC–CA1 synapses between ΔPIX and WT over a range of interpulse intervals (Fig. 3*C*; 50 ms: WT, 214 ± 11%, $n = 9$; ΔPIX, 198 ± 8%, $n = 9$, $p = 0.24$; 100 ms: WT, 183 ± 6%, $n = 9$; ΔPIX, 172 ± 6%, $n = 9$, $p = 0.20$; 150 ms: WT, 165 ± 6%, $n = 9$; ΔPIX, 159 ± 4%, $n = 9$, $p = 0.39$; 200 ms: WT, 152 ± 4%, $n = 9$; ΔPIX, 149 ± 5%, $n = 9$, $p = 0.61$).

Previous work by others found that juvenile AKAP150 knock-out and D36 knock-in mice exhibit normal fEPSP I-O curves and PPR in CA1 extracellular recordings (Lu et al., 2007, 2008; Weisenhaus et al., 2010). However, a subsequent whole-cell recording study found increases in both basal excitatory and inhibitory input to CA1 neurons in these mice as measured by increased frequency of AMPAR-mediated mEPSCs and increased frequency and amplitudes of $GABA_A$ receptor-mediated mIPSCs (Lu et al., 2011). Thus, we next used whole-cell recordings from CA1 neurons in slices to further evaluate basal excitatory and inhibitory transmission in ΔPIX mice. Importantly, we found no significant differences in action potential-dependent AMPAR-mediated spontaneous activity (sEPSCs) or action potential-independent mEPSCs for either mean peak amplitude or mean frequency (Fig. 3*D–G*; sEPSC amplitude: WT, 12.1 ± 0.9 pA, $n = 14$; ΔPIX, 12.6 ± 0.4 pA, $n = 10$, $p = 0.71$; sEPSC frequency: WT, 2.2 ± 0.2 Hz, $n = 14$; ΔPIX, 2.3 ± 0.6 Hz, $n = 10$, $p = 0.90$; mEPSC amplitude: WT, 13.0 ± 0.8 pA, $n = 14$; ΔPIX, 12.1 ± 0.6 pA, $n = 10$, $p = 0.42$; mEPSC frequency: WT, 1.2 ± 0.2 Hz, $n = 14$; ΔPIX, 1.4 ± 0.3 Hz, $n = 10$, $p = 0.68$). Finally, we studied GABA-mediated sIPSC and mIPSC (Fig. 4*A*) events and found no significant differences in mean peak amplitudes or mean frequency (Fig. 4*B–E*; sIPSC amplitude: WT, 61 ± 5 pA, $n = 17$; ΔPIX, 50 ± 5 pA, $n = 17$, $p = 0.15$; sIPSC frequency: WT, 7.5 ± 0.8 Hz, $n = 17$; ΔPIX, 8.9 ± 1.1 Hz, $n = 17$, $p = 0.29$; mIPSC amplitude: WT, 40 ± 4 pA, $n = 9$; ΔPIX, 43 ± 4 pA, $n = 10$, $p = 0.16$; mIPSC frequency: WT, 3.7 ± 0.5 Hz, $n = 9$; ΔPIX, 5.0 ± 0.8 Hz, $n = 10$, $p = 0.68$). Overall, our extracellular and whole-cell recording results suggest that AKAP150ΔPIX mice have essentially normal levels of basal excitatory and inhibitory synaptic input to CA1 neurons.

AKAP150-anchored CaN is required for LTD

Previous studies found LTD impairments at CA1 synapses in forebrain-restricted, conditional CaN knock-out mice and inhibition of LTD by CaN phosphatase inhibitors using a standard low-frequency stimulation (LFS) LTD induction protocol (900 pulses at 1 Hz) (Dudek and Bear, 1992; Mulkey and Malenka, 1992; Mulkey et al., 1994; Zeng et al., 2001). To determine the role of AKAP150-anchored CaN in LTD, we evaluated the ability of several different stimulus protocols to induce LTD at SC–CA1 synapses in ΔPIX mice. Using standard 1 Hz LFS, we found that LTD was readily detectable in WT but absent in ΔPIX mice [Fig. 5*A*,*B*; percentage baseline fEPSP slope: WT, 77 ± 1%, $n = 5$; ΔPIX, 112 ± 9%, $n = 10$ slices, $^{**}p = 0.01$ at $t = 86$ min (56 min after LTD induction)]. LTD was blocked in WT mice in the presence of the antagonist MK-801 confirming that LFS-LTD induction is NMDAR dependent (percentage baseline fEPSP slope 50 min after LTD induction: WT, 76 ± 3%, $n = 5$; WT plus MK-801, 97 ± 7%, $n = 9$). Using a stronger LTD induction protocol that delivers a 1 Hz paired pulse with a 50 ms interpulse interval, which was also shown to be NMDAR dependent in mice (Lee et

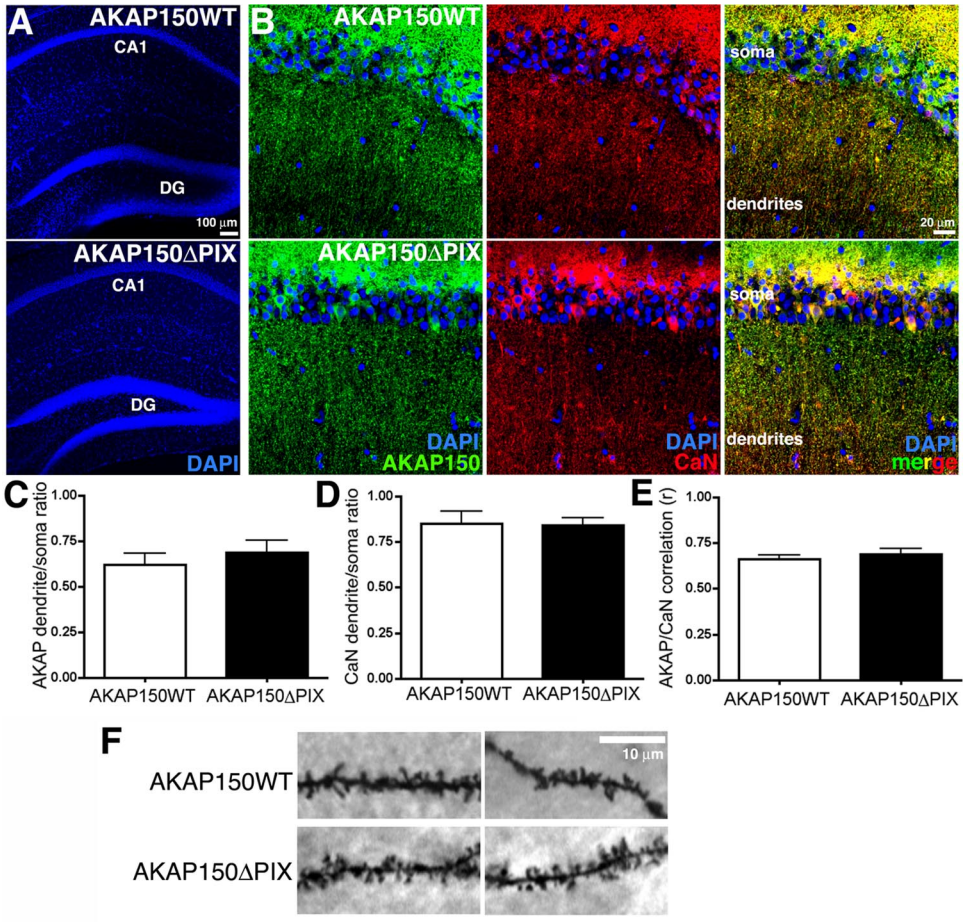

Figure 2. AKAP150ΔPIX mice exhibit normal hippocampal anatomy and localization of AKAP150 and CaN in area CA1. ***A***, Coronal sections from 300-μm-thick acute brain slices prepared from AKAP150WT and AKAP150ΔPIX mice stained with DAPI to visualize nuclei in the cell body layers of the hippocampal CA1 and dentate gyrus (DG) regions. ***B***, Immunostaining of AKAP150 (green), the CaNB regulatory subunit (red), and nuclei (DAPI, blue) in the hippocampal CA1 region of acute brain slices. Colocalization of AKAP150 and CaNB appears yellow in the merge panels. ***C***, ***D***, Quantification of AKAP150 (***C***) and CaNB (***D***) localization in CA1 dendritic versus somatic/cell body areas from ***B*** calculated as dendrite/soma mean fluorescence intensity ratios. ***E***, Relative colocalization of AKAP150 and CaNB in CA1 dendritic areas from ***B*** measured by a fluorescence intensity correlation coefficient (*r*). ***F***, Representative images of Golgi stained dendrites in the CA1 region from WT and ΔPIX mice. Error bars indicate SEM.

al., 2003), LTD was still strongly impaired in ΔPIX compared with WT slices [Fig. 5*C*; percentage baseline fEPSP slope: WT, 64 ± 7%, $n = 7$; ΔPIX, 90 ± 8%, $n = 5$ slices, $^{*}p = 0.036$, at $t =$ 88 min (58 min after LTD induction)].

In conditional CaN knock-out mice, an intermediate stimulation frequency of 10 Hz (900 pulses) induced a slight potentiation that was not seen in WT mice (Zeng et al., 2001). By contrast, for both ΔPIX and WT we found no significant LTP or LTD relative to baseline following 10 Hz stimulation (Fig. 5*D*). However, WT slices showed an initial decrease in fEPSP slope that was not seen for ΔPIX slices using either 10 Hz [Fig. 5*D*; percentage baseline fEPSP slope: WT, 65 ± 6%, $n = 4$; ΔPIX, 91 ± 5.2%, $n =$ 6, $^{**}p = 0.01$, at $t = 22$ min (1 min after LTD induction)] or 1 Hz LFS above (Fig. 5*A*; percentage baseline fEPSP slope: WT, 74 ± 11%, $n = 5$; ΔPIX, 104 ± 10%, $n = 10$, $^{*}p = 0.04$, at 36 min, 1 min after LTD induction). With the stronger 1 Hz PP-LFS, AKAP150ΔPIX mice did exhibit an initial decrease in fEPSP slope, but this decrease was still significantly less than that seen for WT [Fig. 5*C*; percentage baseline fEPSP slope: WT, 42 ± 7%, $n = 7$; ΔPIX, 67 ± 9%, $n = 5$, $^{*}p = 0.04$, at $t = 36$ min (1 min after LTD induction)]. These findings indicate that AKAP150-anchored CaN is acting as a key postsynaptic sensor of NMDAR Ca^{2+} influx to initiate signaling pathways that are required for the induction and expression of LTD.

AKAP150-anchored CaN limits LTP but is not strictly required for synaptic depotentiation

Pharmacologic or genetic inhibition of CaN activity can enhance LTP induced by various forms of high-frequency stimulation (HFS) (Wang and Kelly, 1996, 1997; Winder et al., 1998; Malleret et al., 2001). However, LTP is normal in conditional CaN knock-out animals when induced by standard 1 × 100 Hz, 1 s HFS but is slightly enhanced when using weaker 40 Hz stimulation (Zeng et al., 2001). To test the involvement of AKAP150-anchored CaN in LTP regulation, we next studied LTP in ΔPIX mice using different stimulus frequencies for induction. Using 1 × 100 Hz, 1 s HFS, we found that AKAP150ΔPIX slices expressed significantly enhanced LTP compared with WT [Fig. 6*A*; percentage baseline fEPSP slope: WT, 134 ± 17%, $n = 6$; ΔPIX, 192 ± 16%, $n = 8$, $^{*}p = 0.018$, at $t = 58$ min (38 min after LTP induction)]. In contrast, there was no difference between ΔPIX and WT using 50 Hz, 2 s to induce LTP (Fig. 6*B*). These data for 50 Hz versus 100 Hz indicate that AKAP150-anchored CaN limits the magnitude of LTP following strong but not weaker induction stimuli.

NMDAR-dependent depotentiation of prior LTP, like homosynaptic LTD, is also induced by 1 Hz LFS and involves dephosphorylation of GluA1 Ser831, but not S845 (Lee et al., 2000). To examine whether AKAP150 anchored CaN is also involved in depotentiation, we induced LTP with 100 Hz HFS, recorded for

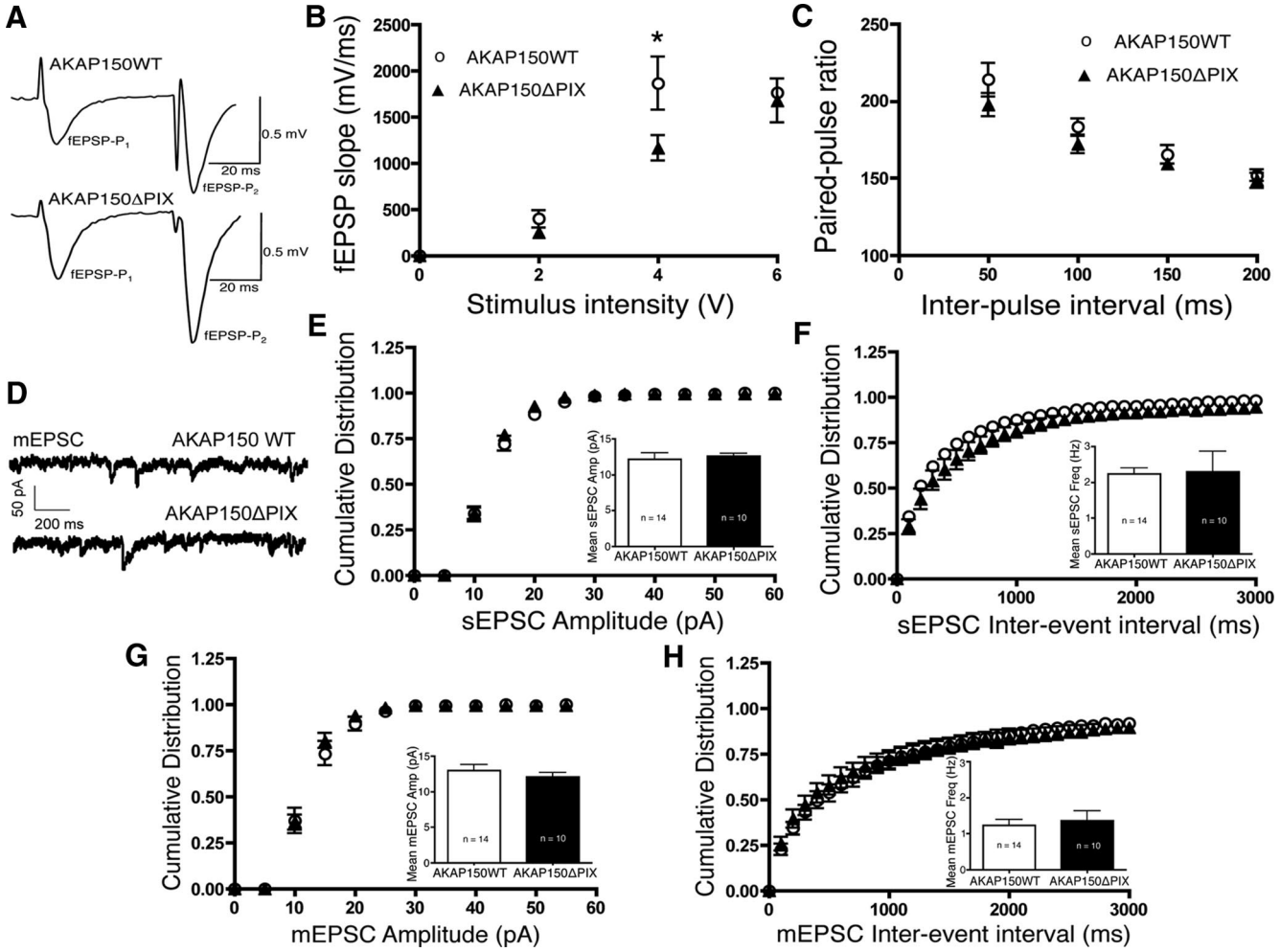

Figure 3. AKAP150ΔPIX mice exhibit normal basal excitatory synaptic transmission in CA1 hippocampal pyramidal neurons. ***A***, Representative fEPSP recordings at SC–CA1 synapses recorded in stratum radiatum of acute hippocampal slices prepared from 2- to 3-week-old AKAP150ΔPIX and WT mice. The fEPSP responses shown are from paired-pulse facilitation ratio (PPR) measurements in ***C*** using an interstimulus interval of 50 ms. ***B***, Input–output curves of fEPSP slope (in millivolts/millisecond) plotted versus stimulus intensity (in volts) for CA1 synapses in AKAP150ΔPIX (filled triangles) and WT (open circles) mice. ***C***, PPR measurements of percentage $fEPSP_2/fEPSP_1$ amplitude for recordings as in ***A*** for ΔPIX and WT mice across a range of different interstimulus intervals. ***D***, Representative whole-cell mEPSC recordings from CA1 pyramidal neurons in acute slices from ΔPIX and WT mice. ***E–H***, Cumulative distribution plots and inset bar graphs (means) of sEPSC amplitudes (in picoamperes) (***E***), sEPSC frequency (interevent interval, means in hertz) (***F***), mEPSC amplitudes (in picoamperes) (***G***), and mEPSC frequency (interevent interval, means in hertz) (***H***) for ΔPIX and WT mice. Error bars indicate SEM. $^*p < 0.05$.

30 min, and then induced depotentiation with 1 Hz LFS (Fig. 6*C*). Both WT and ΔPIX slices exhibited depotentiation; however, while the fEPSP responses for WT slices returned to near the pre-LTP baseline after LFS, the responses in ΔPIX slices remained increased above baseline (Fig. 6*C*). To better compare the relative magnitude of the depotentiation observed in WT and ΔPIX, we renormalized the last 10 min of the LTP responses back to baseline and found that the relative amount of depotentiation was similar for AKAP150ΔPIX and WT (Fig. 6*D*; percentage baseline fEPSP slope: WT, 73 ± 3%, $n = 5$; ΔPIX, 79 ± 4%, $n = 4$, $p = 0.228$). Thus, while some of the expression of LTP in ΔPIX mice is refractory to depotentiation by LFS, AKAP150-anchored CaN is not strictly required for depotentiation.

AKAP150-anchored CaN regulates NMDA-cLTD GluA1 dephosphorylation and removal from synapses

Brief bath application of NMDA produces a form of cLTD that is similar to homosynaptic LTD induced by LFS, and importantly, both of these stimulation methods induce selective dephosphorylation of GluA1 S845, but not S831, through activation of CaN and other phosphatases (Kameyama et al., 1998; Lee et al., 1998). Additionally, GluA1 S845/831A and S845A knock-in mice are deficient in LTD, but S831A mice express normal LTD, further indicating that LTD requires regulation of only S845 phosphorylation (Lee et al., 2003, 2010). Basal levels of GluA1 S845 phosphorylation detected by a phosphospecific antibody were significantly higher (~30–50%) in whole-cell lysates of hippocampal tissue (Fig. 7*A*; GluA1 pS845/GluA1: WT, 0.8 ± 0.2, $n = 8$; ΔPIX, 1.4 ± 0.2, $n = 6$, $^*p = 0.027$) and acute hippocampal slices from AKAP150ΔPIX mice compared with WT (Fig. 7*B*; GluA1 pS845/GluA1: WT, 1.2 ± 0.1, $n = 6$; ΔPIX, 1.6 ± 0.2, $n = 6$, $^*p = 0.027$). Immediately following cLTD (20 μM NMDA; 3 min) treatment of slices, GluA1 S845 phosphorylation (GluA1 pS845/GluA1 normalized to WT $t = 0$) decreased ~45–50% (Fig. 7*C*; WT, 0.50 ± 0.08, $n = 6$; ΔPIX, 0.73 ± 0.09, $n = 6$) for both AKAP150ΔPIX and WT relative to their respective initial levels (WT, 1.00 ± 0.04, $n = 6$; ΔPIX, 1.33 ± 0.13, $n = 6$, $^*p < 0.05$); however, by 60 min after cLTD, S845 phosphorylation recovered completely back to the higher initial level for ΔPIX while remaining ~20% decreased for WT (WT, 0.80 ± 0.06, $n = 6$; ΔPIX,

1.40 ± 0.07, $n = 6$; ***$p < 0.001$). Importantly, AKAP150ΔPIX pS845/GluA1 levels trended above WT levels even at early time points after NMDA treatment and by 30 min were significantly higher than WT, which had recovered very little (WT, 0.59 ± 0.1, $n = 6$; ΔPIX, 1.02 ± 0.06, $n = 6$, **$p < 0.01$). Thus, AKAP150-anchored CaN limits basal GluA1 S845 phosphorylation and is required for efficient and persistent dephosphorylation of this site after NMDA-cLTD.

In cultured rat hippocampal neurons, Ca^{2+}, CaN activity, and the AKAP79/150 CaN anchoring domain are required for the downregulation of AMPAR currents and internalization of AMPAR in response to either acute NMDA receptor activation or inhibition of PKA anchoring and activity (Beattie et al., 2000; Tavalin et al., 2002; Hoshi et al., 2005; Snyder et al., 2005; Bhattacharyya et al., 2009). Thus, we next treated cultured hippocampal neurons from AKAP150ΔPIX and WT mice with NMDA-cLTD (50 μM, 5 min) and assayed for changes in GluA1 synaptic colocalization with PSD-95 by immunostaining (Fig. 8*A*,*B*). As expected, cLTD led to removal of GluA1 from synapses in WT mouse neurons seen by decreased colocalization with PSD-95 within ~8 min of NMDA treatment that persisted for at least 30 min as shown by decreased correlation values [Fig. 8*A*,*C*; GluA1/PSD-95 correlation (*r*): WT control, 0.4 ± 0.03, $n = 10$; NMDA, 0.18 ± 0.09, $n = 10$, **$p = 0.01$]. In contrast, in AKAP150ΔPIX neurons GluA1 postsynaptic colocalization with PSD-95 was unchanged following cLTD treatment even after 30 min [Fig. 8*B*,*C*; GluA1/PSD-95 correlation (*r*): ΔPIX control, 0.33 ± 0.03, $n = 10$; NMDA, 0.34 ± 0.03, $n = 10$, $p = 0.39$]. These results indicate that AKAP150-CaN anchoring is required for AMPAR synaptic removal in NMDA-cLTD.

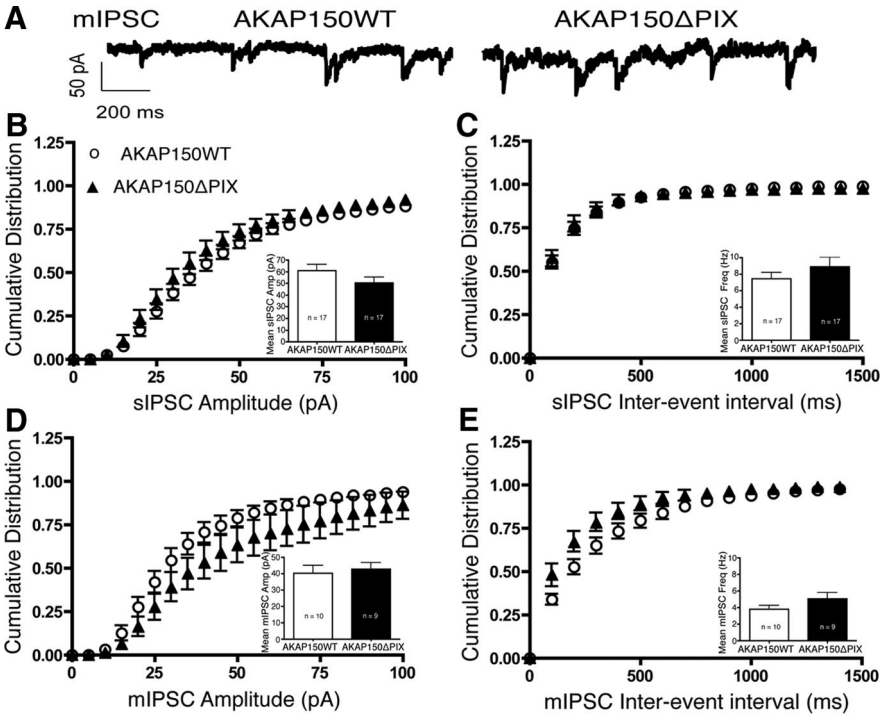

Figure 4. AKAP150ΔPIX mice exhibit normal basal inhibitory synaptic transmission in CA1 hippocampal pyramidal neurons. ***A***, Representative whole-cell mIPSC recordings from CA1 pyramidal neurons in acute slices from AKAP150ΔPIX and WT mice. ***B–E***, Cumulative distribution plots and inset bar graphs (means) for sIPSC amplitudes (in picoamperes) (***B***), sIPSC frequency (interevent interval, means in hertz) (***C***), mIPSC amplitudes (in picoamperes) (***D***), and mIPSC frequency (interevent interval, means in hertz) (***E***) for ΔPIX and WT mice. Error bars indicate SEM.

AKAP150-anchored CaN regulates removal of PSD-95 and AKAP150 from synapses following NMDA-LTD

AMPAR removal from synapses during LTD also involves regulation of receptor tethering to PSD-95 through the AMPAR-associated protein Stargazin. In response to LTD, PSD-95 binding to Stargazin and targeting to the PSD are decreased by activation of protein phosphatases, including CaN (Colledge et al., 2003; Tomita et al., 2005; Kim et al., 2007; Opazo et al., 2010). Accordingly in WT neurons, cLTD led to a rapid ~50% decrease in the intensity of PSD-95 puncta (Fig. 8*A*) that was still evident after 30 min (Fig. 8*A*,*D*; PSD-95 mean intensity: WT control, 380 ± 20, $n = 20$; NMDA, 190 ± 11, $n = 17$; ***$p < 0.001$). However, in ΔPIX neurons, PSD-95 clustering remained unaltered after cLTD (Fig. 8*B*,*D*; PSD-95 mean intensity: ΔPIX control, 340 ± 20, $n = 17$; NMDA, 310 ± 25, $n = 19$, $p = 0.13$). These results indicate that anchoring of CaN to AKAP150 is required for decreased PSD-95 postsynaptic localization after NMDA-cLTD.

AKAP79/150 is targeted to dendritic spines and the PSD by an N-terminal basic region that is palmitoylated on two Cys residues and binds directly to the membrane lipid phosphatidylinositol-4,5-bisphosphate (PIP_2), the actin cytoskeleton, and cadherin adhesion molecules (Dell'Acqua et al., 1998; Gomez et al., 2002; Gorski et al., 2005; Horne and Dell'Acqua, 2007; Keith et al., 2012). LTD leads to loss of AKAP79/150 binding to PSD-95 and cadherins and removal of the AKAP and PKA from synapses (Gomez et al., 2002; Gorski et al., 2005; Smith et al., 2006). LTD-associated loss of AKAP–PKA complexes from spines and the PSD is coincident with, but slightly delayed in time from GluA1 S845 dephosphorylation and endocytosis, and may prevent rephosphorylation of GluA1 (Smith et al., 2006). This AKAP removal from synapses is caused by inhibition of N-terminal targeting interactions through depalmitoylation, phospholipase C cleavage of PIP_2, and CaN-dependent actin depolymerization (Gomez et al., 2002; Horne and Dell'Acqua, 2007; Keith et al., 2012). Thus, we examined whether anchored CaN was required for loss of AKAP150 colocalization with PSD-95 following cLTD. We found that, in contrast to AKAP150WT (Fig. 9*A*), AKAP150ΔPIX protein resisted removal from synapses 30 min after cLTD treatment with increasing doses of NMDA (Fig. 9*B*). Quantification of correlation values for AKAP150 colocalization with PSD-95 revealed that AKAP150ΔPIX required a 70 μM NMDA-cLTD treatment to remove it from synapses, whereas AKAP150WT was efficiently removed by 30 or 50 μM NMDA, as in previous studies in rat neurons (Smith et al., 2006; Horne and Dell'Acqua, 2007; Keith et al., 2012) [Fig. 9*C*; AKAP/PSD-95 correlation (*r*): WT control, 0.35 ± 0.03; 30 μM NMDA, 0.08 ± 0.05 (**$p < 0.01$); 50 μM NMDA, −0.12 ± 0.03 (**$p < 0.01$); 70 μM NMDA, −0.02 ± 0.04 (**$p < 0.01$), $n = 14$–20; ΔPIX control, 0.25 ± 0.02; 30 μM NMDA, 0.27 ± 0.02; 50 μM NMDA, 0.33 ± 0.02; 70 μM NMDA, 0.10 ± 0.06 (*$p < 0.05$); $n = 16$–19]. Thus, AKAP150-anchored CaN is also promoting signaling pathways that contribute to AKAP movement from the PSD during NMDA-cLTD. At 70 μM

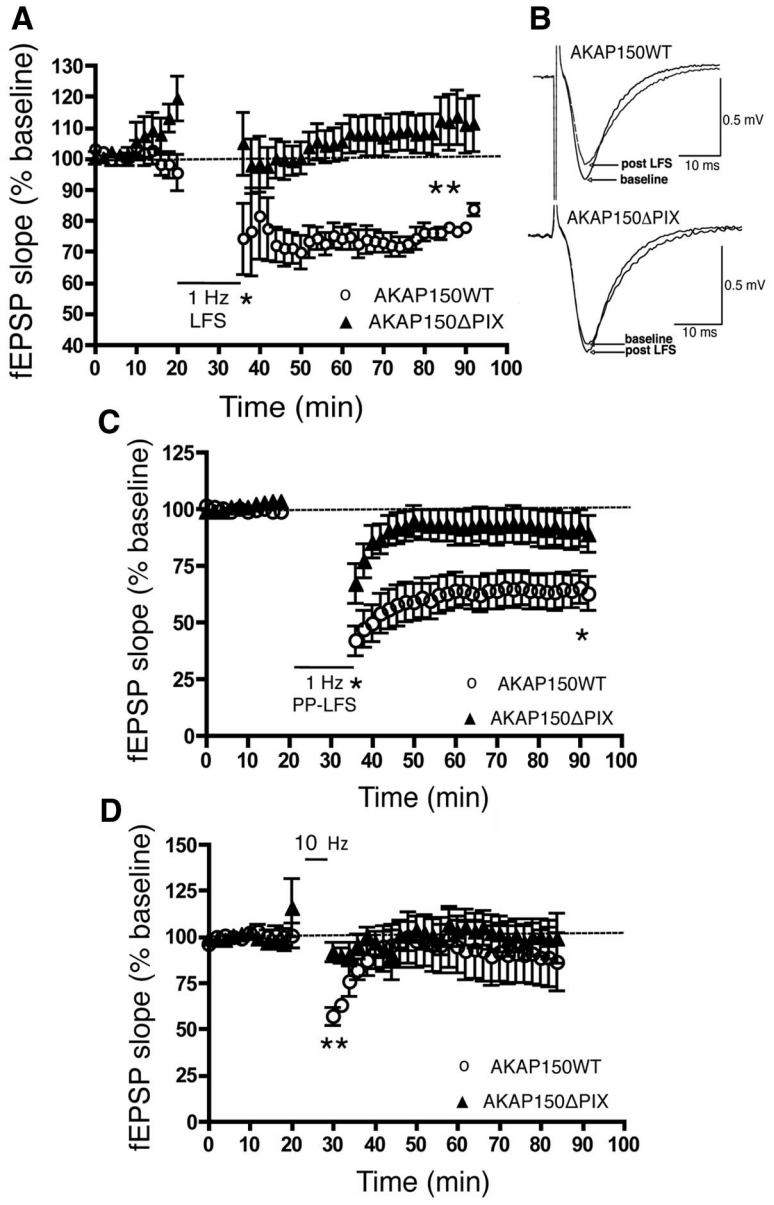

Figure 5. NMDAR-dependent LTD is impaired at CA1 synapses of AKAP150ΔPIX mice. ***A***, One hertz LFS (900 pulses) LTD induction in the SC–CA1 pathway of acute hippocampal slice prepared from 2- to 3-week-old WT (open circles) but not AKAP150ΔPIX mice (filled triangles). fEPSP slope is plotted over time as percentage of the baseline before LFS. ***B***, Representative fEPSP recordings from ***A*** for before and after LFS in WT and ΔPIX mice. ***C***, One hertz PP-LFS (900 paired pulses, 50 ms interpulse interval) induction of LTD in WT but not ΔPIX mice. ***D***, Ten hertz stimulation induction of a transient fEPSP slope depression in WT but not ΔPIX mice. Error bars indicate SEM. $*p < 0.05$, $**p < 0.01$.

NMDA, sufficient Ca^{2+} influx may be generated to efficiently activate unanchored CaN. Consistent with this idea, a previous overexpression study in cultured rat neurons found that an AKAP150 mutant with a larger deletion surrounding the CaN anchoring site moved from spines with 100 μM NMDA treatment (Bhattacharyya et al., 2009).

AKAP150-anchored CaN limits synaptic activity of GluA2-lacking Ca^{2+}-permeable AMPA receptors to promote LTD and constrain LTP

Characterization of GluA1 S845A knock-in mice found that S845 phosphorylation stabilizes a population of homomeric GluA2-lacking receptors in the extrasynaptic plasma membrane where they can exchange in and out of the synapse (He et al., 2009). In addition, it was found that dephosphorylation and endocytosis of this pool of GluA1 is required for LTD, explaining why S845A knock-in mice that lack this receptor pool are deficient in LTD (He et al., 2009; Lee et al., 2010). Thus, the enhanced basal S845 phosphorylation and impaired dephosphorylation and removal of GluA1 we observe for ΔPIX mice could indicate that there is increased synaptic contribution of Ca^{2+}-permeable AMPAR that interferes with LTD expression. To investigate this possibility, we first measured evoked AMPA/NMDA ratios in CA1 neurons using whole-cell recordings (Fig. 10*A*) by dividing the fast AMPAR eEPSC measured either at a membrane holding potential of +40 or −65 mV divided by the slow NMDAR eEPSC measured 70 ms later at +40 mV. While we found no significant difference between ΔPIX and WT animals for the +40 mV AMPA/NMDA ratio (Fig. 10*A*,*B*; +40 AMPA/NMDA ratio: WT, 1.5 ± 0.2, $n = 6$; ΔPIX, 1.9 ± 0.3, $n = 9$; $p = 0.35$), the −65 mV AMPA/NMDA ratio was significantly increased by approximately twofold for ΔPIX (Fig. 10*A*,*C*; −65 AMPA/NMDA +40 ratio: WT, 3.2 ± 0.7, $n = 6$; ΔPIX, 6.4 ± 1.9, $n = 9$; $*p = 0.031$). Since GluA2-lacking AMPARs exhibit pronounced inward rectification, these AMPA/NMDA ratio results suggest that ΔPIX mice may have more Ca^{2+}-permeable AMPARs that increase synaptic inward currents at −65 mV with little impact on outward currents at +40 mV, which are carried predominantly by GluA2-containing receptors. Furthermore, an unchanged +40 mV AMPA/NMDA also suggests that ΔPIX mice have normal NMDAR activity because decreased NMDAR function would increase the +40 and −65 mV ratios equivalently and increased NMDAR activity would change both ratios in the opposite direction as observed. Decreased NMDAR function in ΔPIX mice is also not consistent with our findings of enhanced LTP.

The inward rectification of GluA2-lacking receptors is due to voltage-dependent block of the channel pore at depolarized membrane potentials by intracellular polyamines (Rozov et al., 1998). Since endogenous polyamines can be dialyzed out of the cell over time during whole-cell recording, our AMPA/NMDA ratio measurements (performed without supplementation of intracellular polyamines) may somewhat underestimate changes in AMPAR subunit composition at ΔPIX synapses if polyamine levels decreased enough to allow some outward current through CP-AMPARs. Thus, we next recorded pharmacologically isolated AMPAR eEPSCs with the polyamine spermine present in the intracellular solution to better maintain rectification. While WT CA1 neurons typically displayed robust outward +40 mV and inward −65 mV AMPAR EPSCs, ΔPIX CA1 neurons in general showed reduced outward compared with inward AMPAR currents, with some neurons showing particu-

larly large differences (Fig. 10*D*). Measurements of AMPAR EPSCs across a range of different membrane potentials to obtain a normalized current–voltage relationship (*I–V* curve; Fig. 10*E*) revealed an expected linear *I–V* curve for WT neurons, consistent with the presence of GluA2 in most synaptic receptors, while ΔPIX neurons exhibited clear inward rectification in the *I–V* curve, with significantly decreased outward current measured at +40 mV compared with inward current at −65 mV (Fig. 10*E*; normalized $I_{AMPA+40mV}$: WT, 0.6 ± 0.1, $n = 6$; ΔPIX, 0.19 ± 0.03, $n = 10$, $^{**}p = 0.004$). This approximately threefold increase of inward rectification in ΔPIX compared with WT neurons can also be expressed as a significantly increased AMPA −65/+40 mV EPSC rectification index calculated for each neuron that is consistent with increased levels of GluA2-lacking AMPARs at ΔPIX CA1 synapses (Fig. 10*F*; AMPA EPSC rectification index: WT, 1.5 ± 0.2, $n = 6$; ΔPIX, 5.3 ± 0.8, $n = 11$; $^{**}p = 0.003$) (Stubblefield and Benke, 2010). Since outward AMPAR currents are still clearly measurable for ΔPIX, we can conclude that GluA2-containing receptors are still contributing appreciably to synaptic transmission at ΔPIX synapses; however, based on the increased average rectification index, they may have either been partially replaced by GluA2-lacking receptors at most synapses or perhaps more completely replaced at a subset of synapses.

These whole-cell recording results all point to increased activity of GluA1 homomers in ΔPIX CA1 neurons that could be contributing to LTP enhancement and LTD impairment if these receptors were recruited to synapses and not removed after HFS and LFS, respectively. To explore whether GluA2-lacking receptors are impacting synaptic plasticity in ΔPIX mice, we applied IEM1460, an extracellular polyamine blocker of Ca^{2+}-permeable AMPARs, immediately after LFS induction of LTD or HFS induction of LTP. In WT slices, IEM1460 had no effect on the level of expression of LTD [Fig. 10*G*; percentage baseline fEPSP slope: WT, 77 ± 1%, $n = 5$ slices; IEM WT, 77 ± 9%, $n = 7$ slices, $p = 0.48$ at $t = 86$ min (56 min after LTD induction)] or LTP [Fig. 10*H*; percentage baseline fEPSP slope: IEM WT, 134 ± 4%, $n = 5$ slices; WT, 140 ± 14%, $n = 6$, $p = 0.49$, at $t = 58$ min (38 min after LTP induction)]. In contrast, IEM1460 treatment of ΔPIX slices allowed for expression of significant LTD that was now similar to WT [Fig. 10*G*; percentage baseline fEPSP slope: IEM ΔPIX, 83 ± 4%, $n = 7$ slices; ΔPIX, 112 ± 9%, $n = 10$ slices, $^{*}p = 0.014$ at $t = 86$ min (56 min after LTD induction)] and completely blocked the expression of LTP [Fig. 10*H*; percentage baseline fEPSP slope: IEM ΔPIX, 106 ± 10%, $n = 8$ slices; ΔPIX, 192 ± 16%, $n = 8$, $^{***}p = 0.003$, at $t = 58$ min (38 min after LTP induction)]. Thus, antagonism of GluA2-lacking AMPARs restores normal LTD but inhibits

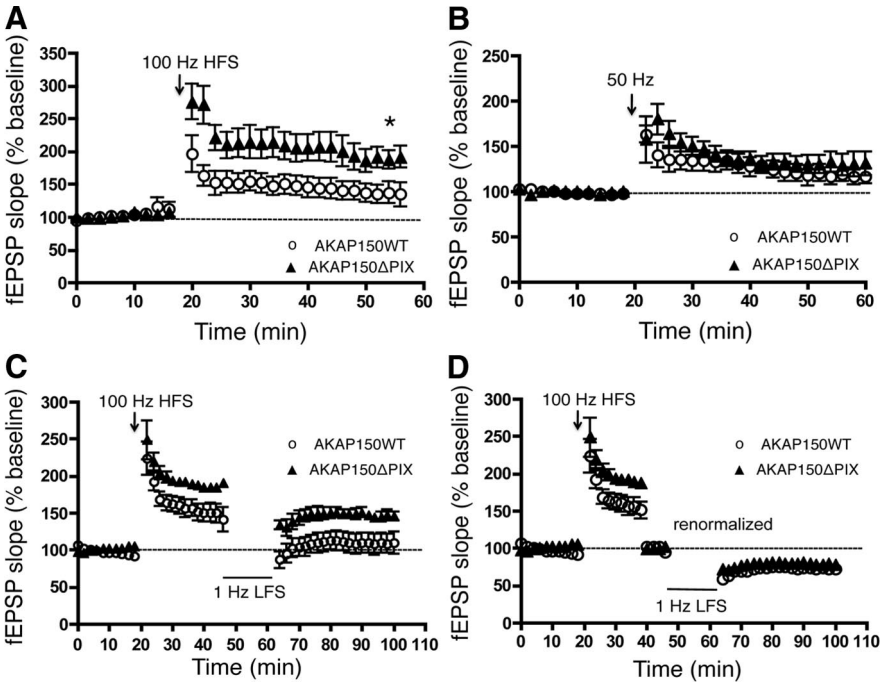

Figure 6. NMDAR-dependent LTP is enhanced at CA1 synapses of AKAP150ΔPIX mice. ***A***, Enhanced 1 × 100 Hz HFS (1 s) induction of LTP in the SC–CA1 pathway of acute hippocampal slices prepared from 2- to 3-week-old AKAP150ΔPIX mice (open circles) compared with WT mice (filled triangles). fEPSP slope is plotted over time as percentage of the baseline before HFS. ***B***, Similar LTP induction with 50 Hz, 2 s stimulation in WT and ΔPIX mice. ***C***, ***D***, LTP (induced 30 min earlier by 1 × 100 Hz HFS) is only partially depotentiated by 1 Hz LFS in ΔPIX compared with WT mice (***C***), but a similar relative percentage depotentiation is observed (***D***). Error bars indicate SEM. $^{*}p < 0.05$.

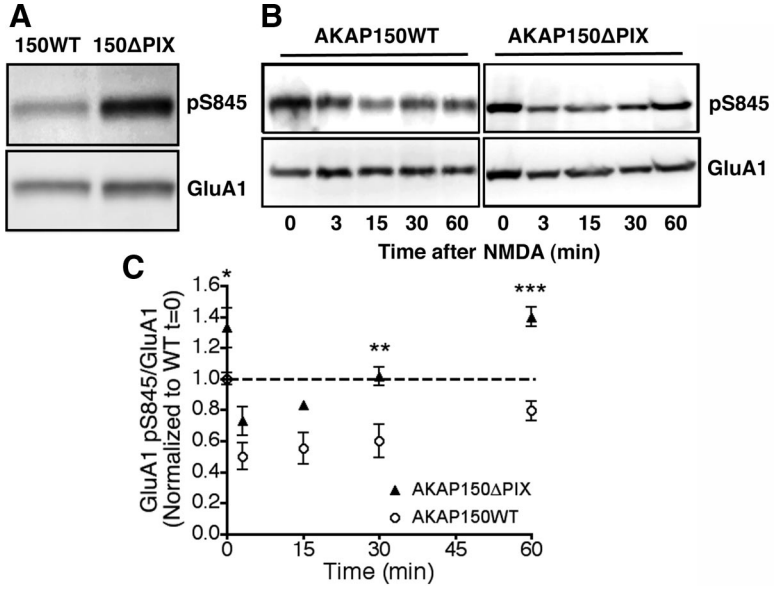

Figure 7. Basal phosphorylation of GluA1 S845 is increased and dephosphorylation following NMDA-cLTD treatment is impaired in AKAP150ΔPIX mice. ***A***, Immunoblots of phospho(p)-S845 and total GluA1 levels in whole-cell extracts of hippocampal tissue from WT and AKAP150ΔPIX mice. ***B***, Immunoblots of pS845 and total GluA1 levels in whole-cell extracts of hippocampal slices from WT and AKAP150ΔPIX mice before ($t = 0$ min) and at the indicated times after NMDA-cLTD (20 μM, 3 min) treatment. ***C***, Quantification of immunoblots as in ***B*** for pS845/GluA1 dephosphorylation over time (normalized to WT $t = 0$ min) after NMDA-cLTD in WT and ΔPIX hippocampal slices. Error bars indicate SEM. $^{*}p < 0.05$, $^{**}p < 0.01$, $^{***}p < 0.001$.

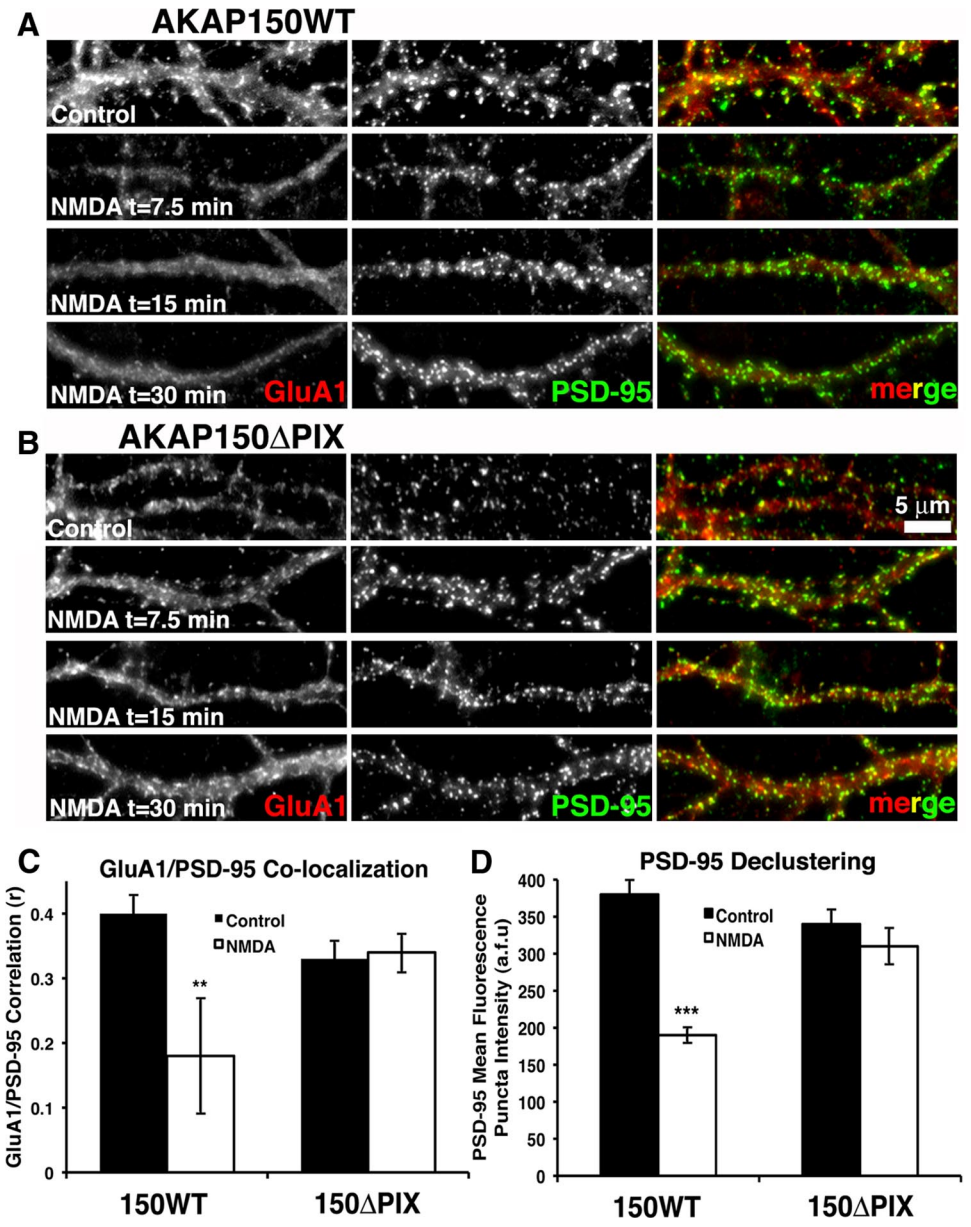

Figure 8. GluA1 and PSD-95 are not removed from synapses following NMDA-cLTD in hippocampal neurons cultured from AKAP150ΔPIX mice. ***A***, ***B***, Immunostaining of GluA1 (red) and PSD-95 (green) in dendrites of hippocampal neurons cultured from AKAP150 WT (***A***) and AKAP150ΔPIX (***B***) mice under control conditions or at the indicated times after NMDA-cLTD treatment (50 μM NMDA, 5 min). Colocalization of GluA1 and PSD-95 puncta appears yellow in the merge panels. ***C***, Quantification of a fluorescence intensity correlation coefficient (*r*) to measure dendritic colocalization of GluA1 and PSD-95 from ***A*** and ***B*** for control conditions and $t = 30$ min after NMDA in WT and AKAP150ΔPIX neurons. ***D***, Quantification of the mean fluorescence intensity of PSD-95 dendritic puncta from ***A*** and ***B*** for control conditions and $t = 30$ min after NMDA in WT and ΔPIX neurons. Error bars indicate SEM. $^{**}p < 0.01$, $^{***}p < 0.001$.

LTP in ΔPIX mice indicating that AKAP150-anchored CaN normally controls bidirectional synaptic plasticity by preventing Ca^{2+}-permeable AMPAR recruitment to synapses where they can interfere with expression of LTD and enhance expression of LTP.

Discussion

We produced a limited knock-in mutation to specifically eliminate CaN anchoring to AKAP150. This knock-in minimized problems associated with complete AKAP150 knock-out, which simultaneously removes multiple and opposing functions (i.e., both PKA and CaN anchoring) and thus limits phenotypic impacts and mechanistic interpretations. Importantly, in ~2- to 3-week-old mice, where synaptic plasticity is normal in AKAP150 knock-outs (Weisenhaus et al., 2010), our characterization of AKAP150ΔPIX mice revealed that CaN anchoring is essential for LTD and constrains LTP. Our findings of impaired LTD and enhanced LTP with AKAP-CaN anchoring disruption are similar to previous studies using less specific genetic or pharmacologic inhibition of CaN activity in hippocampal slices (Wang and Kelly, 1996, 1997; Malleret et al., 2001; Zeng et al., 2001). Thus, our results suggest that most of the important LTD/LTP signaling functions of CaN may be mediated by postsynaptic anchoring to AKAP150. Our findings are also in agreement with previous studies in culture preparations that implicated AKAP79/150-CaN anchoring in regulation of AMPAR activity and endocytosis underlying LTD (Tavalin et al., 2002; Hoshi et al., 2005; Bhattacharyya et al., 2009; Jurado et al., 2010). However, AKAP150ΔPIX mice allowed us to go much further than past studies by using a

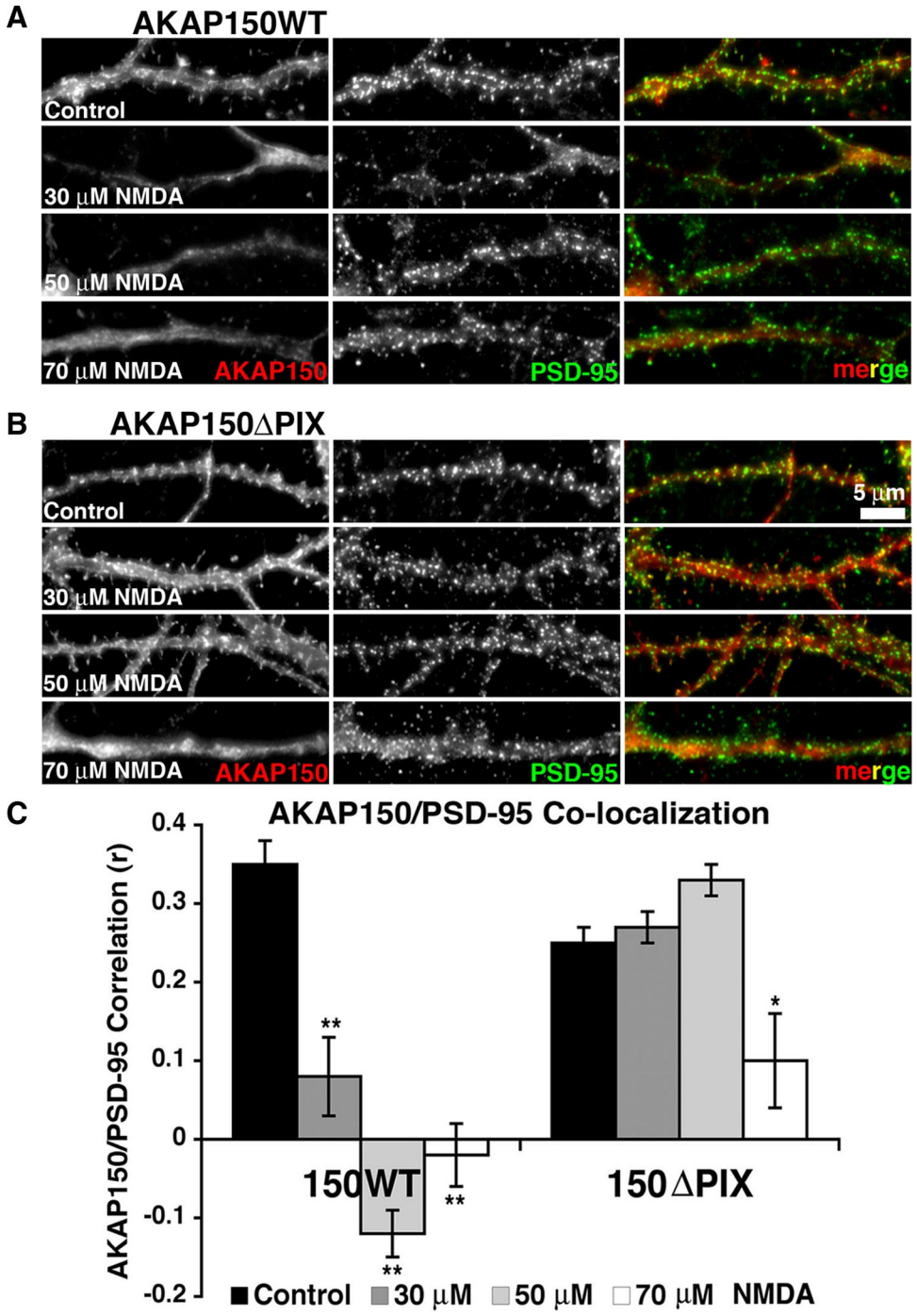

Figure 9. Removal of AKAP150 from synapses following NMDA-cLTD is impaired in hippocampal neurons cultured from AKAP150ΔPIX mice. ***A***, ***B***, Immunostaining of AKAP150 (red) and PSD-95 (green) in dendrites of hippocampal neurons cultured from WT (***A***) and AKAP150ΔPIX (***B***) mice under control conditions or 30 min after cLTD treatment (5 min) with the indicated doses of NMDA. Colocalization of AKAP150 and PSD-95 puncta appears yellow in the merge panels. ***C***, Quantification of a fluorescence intensity correlation coefficient (*r*) to measure dendritic colocalization of AKAP150 and PSD-95 from ***A*** and ***B*** for control conditions and 30 min after treatment with the indicated doses of NMDA in WT and AKAP150ΔPIX neurons. Error bars indicate SEM. $^{*}p < 0.05$, $^{**}p < 0.01$.

combination of electrophysiological, biochemical, and cell biological methods to study the mechanisms by which AKAP-CaN anchoring regulates LTD not only *in vitro* in cultured neurons but also *ex vivo* in hippocampal slices. Using this integrated approach, we discovered a novel role for AKAP-CaN in dephosphorylating GluA1 S845 and limiting the synaptic incorporation of GluA2-lacking Ca^{2+}-permeable AMPARs to regulate not only LTD but also LTP expression.

AKAP150-CaN regulation of AMPAR phosphorylation and subunit composition during LTD

Through its linkage by PSD-95 family MAGUKs (Colledge et al., 2000), AKAP150-anchored CaN is targeted near the C termini of AMPARs and NMDARs, where it is optimally positioned to respond to NMDAR Ca^{2+} influx during LTD induction. In addition, CaN is anchored within 10 nm of PKA on the AKAP (Oliveria et al., 2003), likely allowing this kinase-phosphatase

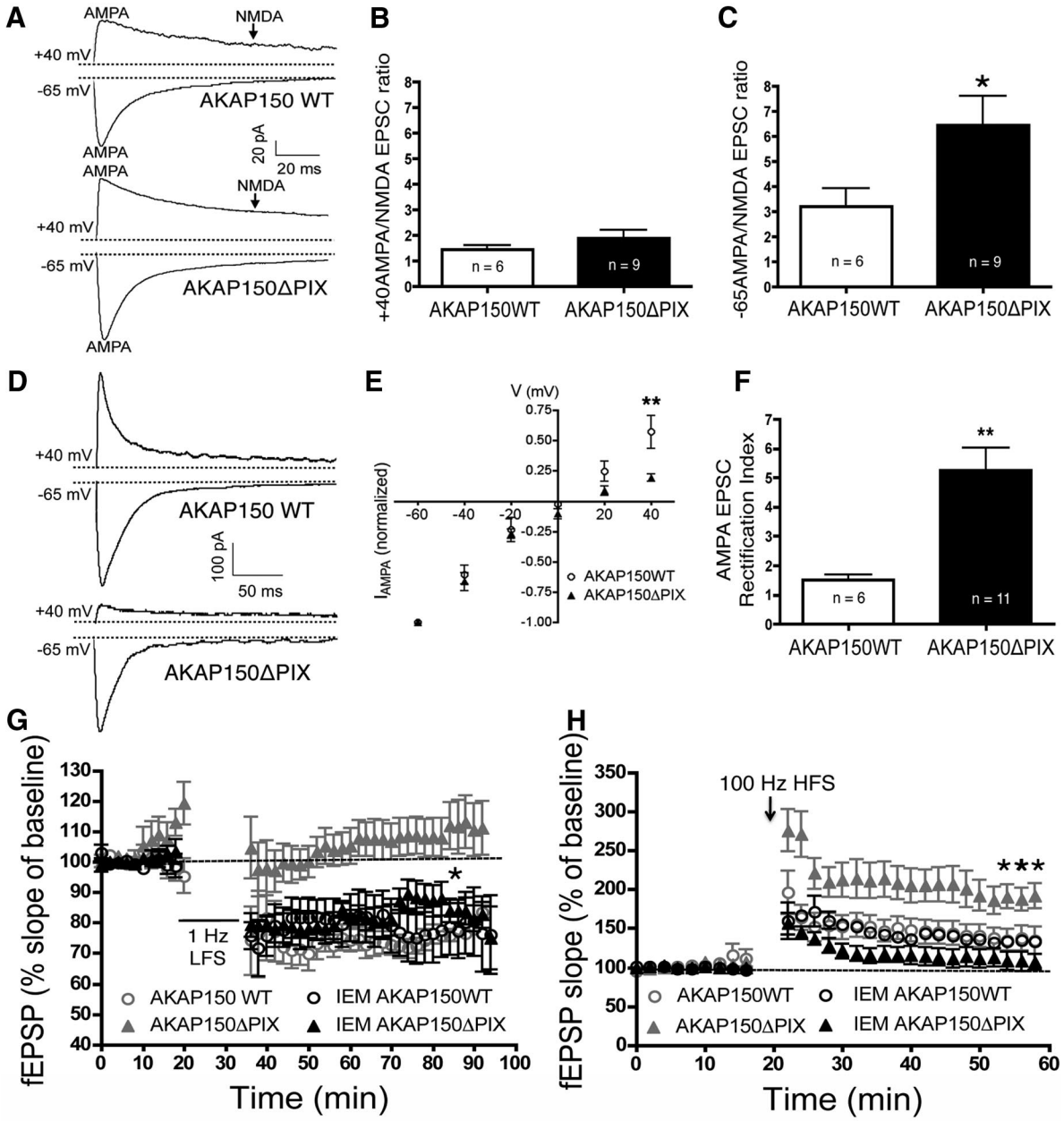

Figure 10. AKAP150ΔPIX mice exhibit increased synaptic activity of GluA2-lacking Ca^{2+}-permeable AMPA receptors that inhibit LTD and enhance LTP expression at CA1 synapses. ***A***, Representative evoked SC–CA1 eEPSC recordings of fast-inward AMPAR current at −65 mV holding potential and fast-outward AMPAR plus slow-outward NMDAR current (arrows) at +40 mV holding potential from CA1 pyramidal neurons in acute hippocampal slices from ΔPIX and WT mice. ***B***, Mean +40 mV AMPA/NMDA eEPSC ratios for ΔPIX and WT mice. ***C***, Mean −65 mV AMPA/NMDA eEPSC ratios for ΔPIX and WT mice. ***D***, Representative pharmacologically isolated AMPAR eEPSC recordings from ΔPIX and WT CA1 neurons with inclusion of spermine in the recording electrode for −65 and +40 mV holding potentials. ***E***, Normalized *I*--*V* curve of pharmacologically isolated AMPAR eEPSCs in ΔPIX and WT CA1 neurons. ***F***, Mean AMPAR eEPSC −65/+40 mV rectification indices for ΔPIX and WT neurons. ***G***, Application of IEM1460 (70 μM) after 1 Hz LFS LTD induction in the SC–CA1 pathway of acute hippocampal slice prepared from 2- to 3-week-old WT (black, open circles) and ΔPIX mice (black, filled triangles). fEPSP slope is plotted over time as percentage of the baseline before LFS. Traces for untreated (control) WT (gray, open circles) and ΔPIX (gray, filled triangles) slices are reproduced from Figure 5*A*. ***H***, Application of IEM1460 after 1 × 100 Hz HFS LTP induction in the SC–CA1 pathway of acute hippocampal slice prepared from 2- to 3-week-old WT (black, open circles) and ΔPIX mice (black, filled triangles). fEPSP slope is plotted over time as percentage of the baseline before HFS. Traces for WT (gray, open circles) and ΔPIX (gray, filled triangles) slices are reproduced from Figure 6*A*. Error bars indicate SEM. $*p < 0.05$, $**p < 0.01$, $***p < 0.001$.

pair to precisely balance each other in regulation of substrates such as GluA1 S845. During LTD, S845 is dephosphorylated by activation of CaN, PP1, and PP2A, removed from synapses, and endocytosed from the extrasynaptic membrane (Lee et al., 1998; Oh et al., 2006; Man et al., 2007; He et al., 2009). Many of these GluA1 receptors may be phosphorylated by PKA before LTD induction (Kameyama et al., 1998; Snyder et al., 2005); however, there is evidence that acute activation of AKAP150 anchored-PKA signaling is also required during LTD (Lu et al., 2008). Regardless, LTD is impaired in GluA1-S845A knock-in mice (Lee et al., 2010), where it was found that S845 phosphorylation stabilizes GluA1 homomers in extrasynaptic locations where they exchange in and out of the synapse but are removed by LTD (He et al., 2009). Importantly, our data show that basal GluA1 S845 phosphorylation levels were significantly higher for ΔPIX compared with WT, and that NMDA-cLTD led to only a par-

tial, transient dephosphorylation of this site (perhaps by unanchored CaN and/or PP1/2A). Consistent with increased GluA1 S845 phosphorylation inhibiting LTD through control of AMPAR subunit composition, we found increased basal activity of GluA2-lacking AMPARs at ΔPIX CA1 synapses and showed that antagonism of these receptors with IEM1460 after LTD induction rescued LTD expression. In contrast, IEM1460 had no effects on LTD expression in WT slices, indicating that GluA2-lacking receptors are either prevented from entering the synapse or are quickly removed by LTD induction as in the study by He et al. (2009). In contrast, for ΔPIX neurons, GluA2-lacking receptors are not removed and likely replace any synaptic GluA2-containing receptors removed during LTD induction to block subsequent expression. These findings further indicate that AKAP150-CaN promotes GluA1 homomer removal, but removal of at least some GluA2-containing receptors does not strictly require CaN anchoring. Thus, the normal function of AKAP-anchored CaN appears to be to dephosphorylate S845 to prevent synaptic incorporation of GluA2-lacking receptors basally and during LTD. Interestingly, our recent published findings indicated that AKAP79/150 palmitoylation targets it to dendritic recycling endosomes in cultured neurons to specifically control GluA1 trafficking and Ca^{2+}-permeable AMPAR synaptic activity (Keith et al., 2012).

GluA1 phosphorylation directly regulates trafficking, but there are other phosphatase substrates, including PSD-95 and Stargazin, that are also involved in synaptic AMPAR removal during LTD. In particular, NMDA-cLTD activation of CaN and PP1/2A negatively regulates PSD-95 postsynaptic clustering and binding to Stargazin to promote AMPAR removal (Colledge et al., 2003; Tomita et al., 2005; Kim et al., 2007; Opazo et al., 2010). CaN activity is also required for cLTD-induced F-actin depolymerization and subsequent disruption of AKAP150 binding to PSD-95 and membranes (Gomez et al., 2002); this uncoupling of AKAP150 from PSD-95 and membranes may prevent PKA rephosphorylation of GluA1 that would promote recycling after LTD (Ehlers, 2000; Snyder et al., 2005; Smith et al., 2006). Importantly, our immunostaining analysis of cultured neurons from AKAP150ΔPIX mice demonstrated that cLTD failed to remove GluA1, PSD-95, and AKAP150 from synapses. Thus, multiple LTD-associated postsynaptic events that control AMPAR localization, including GluA1 dephosphorylation, depend on AKAP150-CaN anchoring.

AKAP150-CaN constrains the potentiated response following LTP induction by limiting synaptic incorporation of Ca^{2+}-permeable AMPA receptors

When AKAP150-CaN anchoring was disrupted in ΔPIX mice, we observed enhanced LTP expression immediately after induction with 1 × 100 Hz HFS as well as continued enhanced potentiation that was blocked by the Ca^{2+}-permeable AMPAR antagonist IEM1460. In contrast, LTP induced in WT mice was insensitive to IEM1460. This finding is consistent with several earlier studies using a variety of different protocols to induce LTP that have in general observed recruitment of GluA2-lacking AMPARs in WT rodents <2 weeks and >4 weeks of age but not in the ~3-week-old age range that we studied (Plant et al., 2006; Lu et al., 2007; Yang et al., 2010) (but see Adesnik and Nicoll, 2007; Gray et al., 2007). In particular, 1 × 100 Hz LTP requires PKA activity, recruits GluA2-lacking AMPARs, and is impaired in PKA-anchoring-deficient AKAP150D36 mice that are >8 weeks of age but not 3–4 weeks of age (Lu et al., 2007). Thus, at the younger age, AKAP-CaN may not only oppose PKA anchored to AKAP150, but also other pools of PKA and perhaps other kinases to limit LTP expression. We did not see enhanced induction or expression of LTP in ΔPIX mice using weaker stimuli of 50 or 10 Hz that enhance potentiation in conditional CaN knock-out mice (Zeng et al., 2001) and GluA1 S831,845D mice that mimic constitutive GluA1 phosphorylation (Makino et al., 2011). These differences could be due to age differences; CaN knock-out and S831,845D mice were studied at older ages of 4–6 weeks. However, our results for ΔPIX mice are similar to those in slices from older mice using a genetically encoded inhibitor to partially block CaN activity (Malleret et al., 2001). Nonetheless, our current results could also indicate that AKAP anchored-CaN plays a more important role in limiting the strength of potentiated response after LTP by opposing phosphorylation of S845 and regulating AMPAR subunit composition rather than in setting the induction threshold, which may involve other pools of CaN and additional substrates.

Interestingly, in ΔPIX mice, we found that LFS-LTD was impaired, but the same LFS protocol significantly depotentiated the enhanced LTP. While LTD and depotentiation are sensitive to genetic manipulations of CaN and PKA expression, their underlying signaling mechanisms are distinct (Brandon et al., 1995; Zhuo et al., 1999; Yang et al., 2009). LTD causes dephosphorylation of the GluA1 S845 PKA site, while depotentiation triggers dephosphorylation of the GluA1 S831 CaMKII/PKC site (Lee et al., 2000). In addition, forebrain-specific CaN knock-out mice, like our ΔPIX mice, exhibit a lack of LTD but maintain normal depotentiation (Zeng et al., 2001). Thus, while AKAP150-anchored CaN is clearly involved in S845 dephosphorylation in LTD, it may be redundant with other phosphatase pathways that dephosphorylate S831 during depotentiation. These findings reinforce that AKAP150-CaN is very specifically targeted to regulate S845, and suggest that the amount of LTP that is refractory to depotentiation in ΔPIX mice is likely due to an inability to dephosphorylate S845 and fully suppress the activity of IEM-sensitive GluA2-lacking receptors that are aberrantly recruited during LTP. Interestingly, past work in heterologous cells demonstrated that negative regulation of recombinant GluA1 currents by AKAP79 involved dephosphorylation of S845 but not S831, required anchored CaN, and was opposed by anchored PKA (Dell'Acqua et al., 2002; Tavalin et al., 2002; Hoshi et al., 2005). In addition, peptide-mediated inhibition of PKA anchoring or activity caused a very similar decrease in AMPAR currents in hippocampal neurons that was mediated by CaN activation in part by Ca^{2+} influx through Ca^{2+}-permeable AMPARs (Rosenmund et al., 1994; Tavalin et al., 2002). Thus, these earlier studies hinted at a role for AKAP79/150-anchored CaN in regulation of Ca^{2+}-permeable GluA1 homomers that our results here now clearly establish as a key mechanism that maintains bidirectional synaptic plasticity in the hippocampus. In the future, it will be interesting to determine whether AKAP-anchored CaN also controls Ca^{2+}-permeable AMPAR activity in response to neuronal insults including seizures and ischemia (Liu and Zukin, 2007).

References

Adesnik H, Nicoll RA (2007) Conservation of glutamate receptor 2-containing AMPA receptors during long-term potentiation. J Neurosci 27:4598–4602.

Ashby MC, De La Rue SA, Ralph GS, Uney J, Collingridge GL, Henley JM (2004) Removal of AMPA receptors (AMPARs) from synapses is preceded by transient endocytosis of extrasynaptic AMPARs. J Neurosci 24:5172–5176.

Banke TG, Bowie D, Lee H, Huganir RL, Schousboe A, Traynelis SF (2000) Control of GluR1 AMPA receptor function by cAMP-dependent protein kinase. J Neurosci 20:89–102.

Beattie EC, Carroll RC, Yu X, Morishita W, Yasuda H, von Zastrow M, Malenka RC (2000) Regulation of AMPA receptor endocytosis by a signaling mechanism shared with LTD. Nat Neurosci 3:1291–1300.

Bhattacharyya S, Biou V, Xu W, Schlüter O, Malenka RC (2009) A critical role for PSD-95/AKAP interactions in endocytosis of synaptic AMPA receptors. Nat Neurosci 12:172–181.

Brandao KE, Dell'Acqua ML, Levinson SR (2012) A-kinase anchoring protein 150 expression in a specific subset of TRPV1- and CaV 1.2-positive nociceptive rat dorsal root ganglion neurons. J Comp Neurol 520:81–99.

Brandon EP, Zhuo M, Huang YY, Qi M, Gerhold KA, Burton KA, Kandel ER, McKnight GS, Idzerda RL (1995) Hippocampal long-term depression and depotentiation are defective in mice carrying a targeted disruption of the gene encoding the RIb subunit of cAMP-dependent protein kinase. Proc Natl Acad Sci U S A 92:8851–8855.

Colledge M, Dean RA, Scott GK, Langeberg LK, Huganir RL, Scott JD (2000) Targeting of PKA to glutamate receptors through a MAGUK-AKAP complex. Neuron 27:107–119.

Colledge M, Snyder EM, Crozier RA, Soderling JA, Jin Y, Langeberg LK, Lu H, Bear MF, Scott JD (2003) Ubiquitination regulates PSD-95 degradation and AMPA receptor surface expression. Neuron 40:595–607.

Dell'Acqua ML, Faux MC, Thorburn J, Thorburn A, Scott JD (1998) Membrane-targeting sequences on AKAP79 bind phosphatidylinositol-4,5-bisphosphate. EMBO J 17:2246–2260.

Dell'Acqua ML, Dodge KL, Tavalin SJ, Scott JD (2002) Mapping the protein phosphatase-2B anchoring site on AKAP79. Binding and inhibition of phosphatase activity are mediated by residues 315–360. J Biol Chem 277:48796–48802.

Dudek SM, Bear MF (1992) Homosynaptic long-term depression in area CA1 of hippocampus and effects of *N*-methyl-D-aspartate receptor blockade. Proc Natl Acad Sci U S A 89:4363–4367.

Ehlers MD (2000) Reinsertion or degradation of AMPA receptors determined by activity-dependent endocytic sorting. Neuron 28:511–525.

Esteban JA, Shi SH, Wilson C, Nuriya M, Huganir RL, Malinow R (2003) PKA phosphorylation of AMPA receptor subunits controls synaptic trafficking underlying plasticity. Nat Neurosci 6:136–143.

Gomez LL, Alam S, Smith KE, Horne E, Dell'Acqua ML (2002) Regulation of A-kinase anchoring protein 79/150-cAMP-dependent protein kinase postsynaptic targeting by NMDA receptor activation of calcineurin and remodeling of dendritic actin. J Neurosci 22:7027–7044.

Gorski JA, Gomez LL, Scott JD, Dell'Acqua ML (2005) Association of an A-kinase-anchoring protein signaling scaffold with cadherin adhesion molecules in neurons and epithelial cells. Mol Biol Cell 16:3574–3590.

Gray EE, Fink AE, Sariñana J, Vissel B, O'Dell TJ (2007) Long-term potentiation in the hippocampal CA1 region does not require insertion and activation of GluR2-lacking AMPA receptors. J Neurophysiol 98:2488–2492.

Guire ES, Oh MC, Soderling TR, Derkach VA (2008) Recruitment of calcium-permeable AMPA receptors during synaptic potentiation is regulated by CaM-kinase I. J Neurosci 28:6000–6009.

He K, Song L, Cummings LW, Goldman J, Huganir RL, Lee HK (2009) Stabilization of Ca^{2+}-permeable AMPA receptors at perisynaptic sites by GluR1–S845 phosphorylation. Proc Natl Acad Sci U S A 106:20033–20038.

Horne EA, Dell'Acqua ML (2007) Phospholipase C is required for changes in postsynaptic structure and function associated with NMDA receptor-dependent long-term depression. J Neurosci 27:3523–3534.

Hoshi N, Langeberg LK, Scott JD (2005) Distinct enzyme combinations in AKAP signalling complexes permit functional diversity. Nat Cell Biol 7:1066–1073.

Hoskison MM, Yanagawa Y, Obata K, Shuttleworth CW (2007) Calcium-dependent NMDA-induced dendritic injury and MAP2 loss in acute hippocampal slices. Neuroscience 145:66–79.

Hsieh H, Boehm J, Sato C, Iwatsubo T, Tomita T, Sisodia S, Malinow R (2006) AMPAR removal underlies Abeta-induced synaptic depression and dendritic spine loss. Neuron 52:831–843.

Jurado S, Biou V, Malenka RC (2010) A calcineurin/AKAP complex is required for NMDA receptor-dependent long-term depression. Nat Neurosci 13:1053–1055.

Kameyama K, Lee HK, Bear MF, Huganir RL (1998) Involvement of a postsynaptic protein kinase A substrate in the expression of homosynaptic long-term depression. Neuron 21:1163–1175.

Keith DJ, Sanderson JL, Gibson ES, Woolfrey KM, Robertson HR, Olszewski K, Kang R, El-Husseini A, Dell'Acqua ML (2012) Palmitoylation of A-kinase anchoring protein 79/150 regulates dendritic endosomal targeting and synaptic plasticity mechanisms. J Neurosci 32:7119–7136.

Kim MJ, Futai K, Jo J, Hayashi Y, Cho K, Sheng M (2007) Synaptic accumulation of PSD-95 and synaptic function regulated by phosphorylation of serine-295 of PSD-95. Neuron 56:488–502.

Lee HK, Kameyama K, Huganir RL, Bear MF (1998) NMDA induces long-term synaptic depression and dephosphorylation of the GluR1 subunit of AMPA receptors in hippocampus. Neuron 21:1151–1162.

Lee HK, Barbarosie M, Kameyama K, Bear MF, Huganir RL (2000) Regulation of distinct AMPA receptor phosphorylation sites during bidirectional synaptic plasticity. Nature 405:955–959.

Lee HK, Takamiya K, Han JS, Man H, Kim CH, Rumbaugh G, Yu S, Ding L, He C, Petralia RS, Wenthold RJ, Gallagher M, Huganir RL (2003) Phosphorylation of the AMPA receptor GluR1 subunit is required for synaptic plasticity and retention of spatial memory. Cell 112:631–643.

Lee HK, Takamiya K, He K, Song L, Huganir RL (2010) Specific roles of AMPA receptor subunit GluR1 (GluA1) phosphorylation sites in regulating synaptic plasticity in the CA1 region of hippocampus. J Neurophysiol 103:479–489.

Li H, Rao A, Hogan PG (2011) Interaction of calcineurin with substrates and targeting proteins. Trends Cell Biol 21:91–103.

Li H, Pink MD, Murphy JG, Stein A, Dell'Acqua ML, Hogan PG (2012) Balanced interactions of calcineurin with AKAP79 regulate Ca^{2+}-calcineurin-NFAT signaling. Nat Struct Mol Biol 19:337–345.

Liu SJ, Zukin RS (2007) Ca^{2+}-permeable AMPA receptors in synaptic plasticity and neuronal death. Trends Neurosci 30:126–134.

Lu Y, Allen M, Halt AR, Weisenhaus M, Dallapiazza RF, Hall DD, Usachev YM, McKnight GS, Hell JW (2007) Age-dependent requirement of AKAP150-anchored PKA and GluR2-lacking AMPA receptors in LTP. EMBO J 26:4879–4890.

Lu Y, Zhang M, Lim IA, Hall DD, Allen M, Medvedeva Y, McKnight GS, Usachev YM, Hell JW (2008) AKAP150-anchored PKA activity is important for LTD during its induction phase. J Physiol 586:4155–4164.

Lu Y, Zha XM, Kim EY, Schachtele S, Dailey ME, Hall DD, Strack S, Green SH, Hoffman DA, Hell JW (2011) A kinase anchor protein 150 (AKAP150)-associated protein kinase A limits dendritic spine density. J Biol Chem 286:26496–26506.

Makino H, Malinow R (2009) AMPA receptor incorporation into synapses during LTP: the role of lateral movement and exocytosis. Neuron 64:381–390.

Makino Y, Johnson RC, Yu Y, Takamiya K, Huganir RL (2011) Enhanced synaptic plasticity in mice with phosphomimetic mutation of the GluA1 AMPA receptor. Proc Natl Acad Sci U S A 108:8450–8455.

Malleret G, Haditsch U, Genoux D, Jones MW, Bliss TV, Vanhoose AM, Weitlauf C, Kandel ER, Winder DG, Mansuy IM (2001) Inducible and reversible enhancement of learning, memory, and long-term potentiation by genetic inhibition of calcineurin. Cell 104:675–686.

Man HY, Sekine-Aizawa Y, Huganir RL (2007) Regulation of α-amino-3-hydroxy-5-methyl-4-isoxazolepropionic acid receptor trafficking through PKA phosphorylation of the Glu receptor 1 subunit. Proc Natl Acad Sci U S A 104:3579–3584.

Miyakawa T, Leiter LM, Gerber DJ, Gainetdinov RR, Sotnikova TD, Zeng H, Caron MG, Tonegawa S (2003) Conditional calcineurin knockout mice exhibit multiple abnormal behaviors related to schizophrenia. Proc Natl Acad Sci U S A 100:8987–8992.

Mulkey RM, Malenka RC (1992) Mechanisms underlying induction of homosynaptic long-term depression in area CA1 of the hippocampus. Neuron 9:967–975.

Mulkey RM, Herron CE, Malenka RC (1993) An essential role for protein phosphatases in hippocampal long-term depression. Science 261:1051–1055.

Mulkey RM, Endo S, Shenolikar S, Malenka RC (1994) Involvement of a calcineurin/inhibitor-1 phosphatase cascade in hippocampal long-term depression. Nature 369:486–488.

Oh MC, Derkach VA, Guire ES, Soderling TR (2006) Extrasynaptic membrane trafficking regulated by GluR1 serine 845 phosphorylation primes AMPA receptors for long-term potentiation. J Biol Chem 281:752–758.

Oliveria SF, Gomez LL, Dell'Acqua ML (2003) Imaging kinase–AKAP79–phosphatase scaffold complexes at the plasma membrane in living cells using FRET microscopy. J Cell Biol 160:101–112.

Oliveria SF, Dell'Acqua ML, Sather WA (2007) AKAP79/150 anchoring of

calcineurin controls neuronal L-type Ca^{2+} channel activity and nuclear signaling. Neuron 55:261–275.

Opazo P, Labrecque S, Tigaret CM, Frouin A, Wiseman PW, De Koninck P, Choquet D (2010) CaMKII triggers the diffusional trapping of surface AMPARs through phosphorylation of Stargazin. Neuron 67:239–252.

Petrini EM, Lu J, Cognet L, Lounis B, Ehlers MD, Choquet D (2009) Endocytic trafficking and recycling maintain a pool of mobile surface AMPA receptors required for synaptic potentiation. Neuron 63:92–105.

Plant K, Pelkey KA, Bortolotto ZA, Morita D, Terashima A, McBain CJ, Collingridge GL, Isaac JT (2006) Transient incorporation of native GluR2-lacking AMPA receptors during hippocampal long-term potentiation. Nat Neurosci 9:602–604.

Qian H, Matt L, Zhang M, Nguyen M, Patriarchi T, Koval OM, Anderson ME, He K, Lee HK, Hell JW (2012) beta2-Adrenergic receptor supports prolonged theta tetanus-induced LTP. J Neurophysiol 107:2703–2712.

Robertson HR, Gibson ES, Benke TA, Dell'Acqua ML (2009) Regulation of postsynaptic structure and function by an A-kinase anchoring protein-membrane-associated guanylate kinase scaffolding complex. J Neurosci 29:7929–7943.

Rosenmund C, Carr DW, Bergeson SE, Nilaver G, Scott JD, Westbrook GL (1994) Anchoring of protein kinase A is required for modulation of AMPA/kainate receptors on hippocampal neurons. Nature 368:853–856.

Rozov A, Zilberter Y, Wollmuth LP, Burnashev N (1998) Facilitation of currents through rat Ca^{2+}-permeable AMPA receptor channels by activity-dependent relief from polyamine block. J Physiol 511:361–377.

Sanderson JL, Dell'Acqua ML (2011) AKAP signaling complexes in regulation of excitatory synaptic plasticity. Neuroscientist 17:321–336.

Scott-McKean JJ, Costa AC (2011) Exaggerated NMDA mediated LTD in a mouse model of Down syndrome and pharmacological rescuing by memantine. Learn Mem 18:774–778.

Shankar GM, Bloodgood BL, Townsend M, Walsh DM, Selkoe DJ, Sabatini BL (2007) Natural oligomers of the Alzheimer amyloid-β protein induce reversible synapse loss by modulating an NMDA-type glutamate receptor-dependent signaling pathway. J Neurosci 27:2866–2875.

Shuttleworth CW, Connor JA (2001) Strain-dependent differences in calcium signaling predict excitotoxicity in murine hippocampal neurons. J Neurosci 21:4225–4236.

Siarey RJ, Carlson EJ, Epstein CJ, Balbo A, Rapoport SI, Galdzicki Z (1999) Increased synaptic depression in the Ts65Dn mouse, a model for mental retardation in Down syndrome. Neuropharmacology 38:1917–1920.

Smith KE, Gibson ES, Dell'Acqua ML (2006) cAMP-dependent protein kinase postsynaptic localization regulated by NMDA receptor activation through translocation of an A-kinase anchoring protein scaffold protein. J Neurosci 26:2391–2402.

Snyder EM, Colledge M, Crozier RA, Chen WS, Scott JD, Bear MF (2005) Role for A kinase-anchoring proteins (AKAPS) in glutamate receptor trafficking and long term synaptic depression. J Biol Chem 280:16962–16968.

Stubblefield EA, Benke TA (2010) Distinct AMPA-type glutamatergic synapses in developing rat CA1 hippocampus. J Neurophysiol 104:1899–1912.

Tavalin SJ, Colledge M, Hell JW, Langeberg LK, Huganir RL, Scott JD (2002) Regulation of GluR1 by the A-kinase anchoring protein 79 (AKAP79) signaling complex shares properties with long-term depression. J Neurosci 22:3044–3051.

Tomita S, Stein V, Stocker TJ, Nicoll RA, Bredt DS (2005) Bidirectional synaptic plasticity regulated by phosphorylation of stargazin-like TARPs. Neuron 45:269–277.

Tunquist BJ, Hoshi N, Guire ES, Zhang F, Mullendorff K, Langeberg LK, Raber J, Scott JD (2008) Loss of AKAP150 perturbs distinct neuronal processes in mice. Proc Natl Acad Sci U S A 105:12557–12562.

Wang JH, Kelly PT (1996) The balance between postsynaptic Ca^{2+}-dependent protein kinase and phosphatase activities controlling synaptic strength. Learn Mem 3:170–181.

Wang JH, Kelly PT (1997) Postsynaptic calcineurin activity downregulates synaptic transmission by weakening intracellular Ca^{2+} signaling mechanisms in hippocampal CA1 neurons. J Neurosci 17:4600–4611.

Weisenhaus M, Allen ML, Yang L, Lu Y, Nichols CB, Su T, Hell JW, McKnight GS (2010) Mutations in AKAP5 disrupt dendritic signaling complexes and lead to electrophysiological and behavioral phenotypes in mice. PLoS One 5:e10325.

Winder DG, Mansuy IM, Osman M, Moallem TM, Kandel ER (1998) Genetic and pharmacological evidence for a novel, intermediate phase of long-term potentiation suppressed by calcineurin. Cell 92:25–37.

Yang Y, Wang XB, Frerking M, Zhou Q (2008) Delivery of AMPA receptors to perisynaptic sites precedes the full expression of long-term potentiation. Proc Natl Acad Sci U S A 105:11388–11393.

Yang Y, Takeuchi K, Rodenas-Ruano A, Takayasu Y, Bennett MV, Zukin RS (2009) Developmental switch in requirement for PKA RIIbeta in NMDA-receptor-dependent synaptic plasticity at Schaffer collateral to CA1 pyramidal cell synapses. Neuropharmacology 56:56–65.

Yang Y, Wang XB, Zhou Q (2010) Perisynaptic GluR2-lacking AMPA receptors control the reversibility of synaptic and spines modifications. Proc Natl Acad Sci U S A 107:11999–12004.

Zeng H, Chattarji S, Barbarosie M, Rondi-Reig L, Philpot BD, Miyakawa T, Bear MF, Tonegawa S (2001) Forebrain-specific calcineurin knockout selectively impairs bidirectional synaptic plasticity and working/episodic-like memory. Cell 107:617–629.

Zhuo M, Zhang W, Son H, Mansuy I, Sobel RA, Seidman J, Kandel ER (1999) A selective role of calcineurin aalpha in synaptic depotentiation in hippocampus. Proc Natl Acad Sci U S A 96:4650–4655.